1 **Spatial-temporal distribution, photoreactivity and environmental**

2 **control of dissolved organic matter in the sea-surface microlayer of**

3 **the eastern marginal seas of China**

4 Lin Yang [a], Jing Zhang [a, c, *], Anja Engel [d], Gui-Peng Yang [a, b, c, *]

5 [a] Frontiers Science Center for Deep Ocean Multispheres and Earth System, and Key Laboratory of

6 Marine Chemistry Theory and Technology, Ministry of Education, Ocean University of China,

7 Qingdao 266100, China

8 [b] Laboratory for Marine Ecology and Environmental Science, Qingdao National Laboratory for

9 Marine Science and Technology, Qingdao 266237, China

10 [c] Institute of Marine Chemistry, Ocean University of China, Qingdao 266100, China

11 [d] GEOMAR Helmholtz Centre for Ocean Research, 24105 Kiel, Germany

[*] Corresponding authors. Key Laboratory of Marine Chemistry Theory and Technology, Ministry of Education, Ocean University of China, Qingdao 266100, China

E-mail addresses: zhangjouc@ouc.edu.cn (J. Zhang), gpyang@ouc.edu.cn (G.-P. Yang)
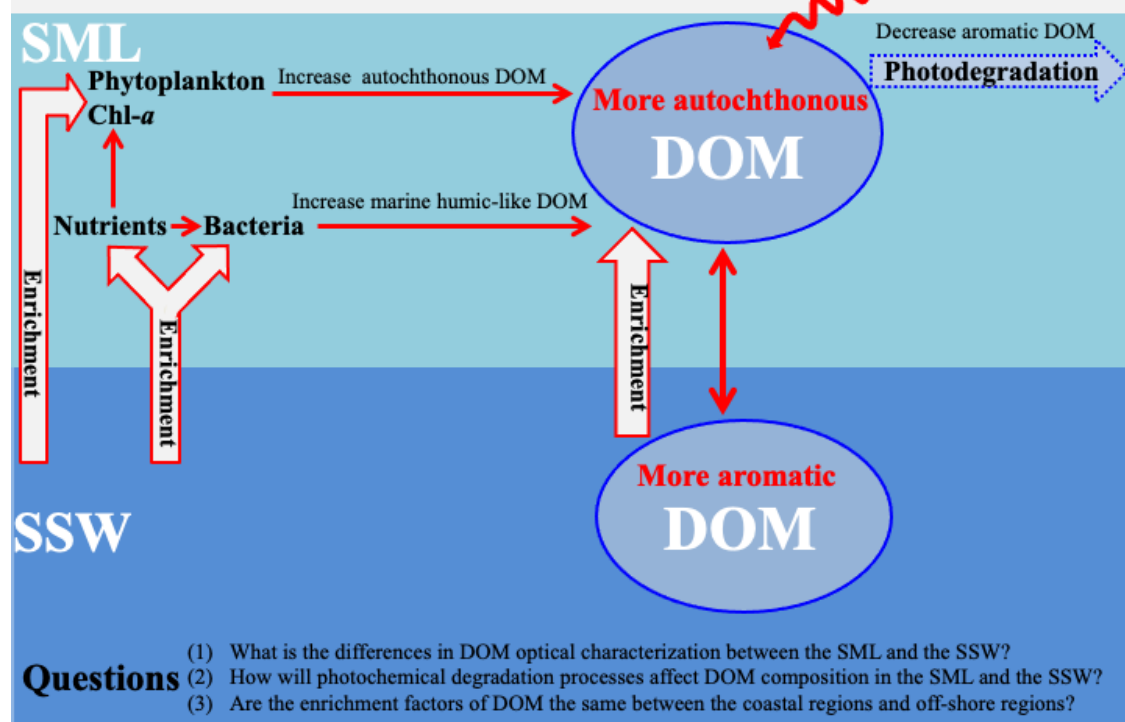
13   Graphical Abstract

14   **Abstract**

15   As the boundary interface between the atmosphere and ocean, the sea-surface microlayer (SML)

16   plays a significant role in the biogeochemical cycles of dissolved organic matter (DOM) and

17   macronutrients in marine environments. In our study, the optical properties of DOM were compared

18   between the SSW and the SML during spring, summer and winter in the East China Sea (ECS) and the

19   Yellow Sea (YS), photoexposure experiments were design to compare photochemical degradation

20   processes of DOM between the SML and the SSW. Chromophoric DOM (CDOM), fluorescent DOM,

21   dissolved organic carbon, chlorophyll a, picoplankton, nutrients, and bacteria were frequently enriched

22   in the SML. The enrichment factors (EFs) of tryptophan-like component 4 was significantly higher

23   than other fluorescence components; the longer wavelength absorption values of CDOM showed

24   higher EFs in the SML, and the more significant relationship between CDOM and Chl-a in the SML,

25   indicating that autochthonous DOM was more strongly enriched in the SML than the terrestrial DOM.

26   We find that higher EFs were generally observed in the SML in the off-shore regions than in the

27   coastal regions, and CDOM in the SML is photobleached less after relatively strong irradiation, as also

28   indicated by the lower percentages of humic-like DOM and lower specific UV absorbance values

29   ($SUVA_{254}$) in the SML than the subsurface water (SSW). Compared to the SSW, the elevated nutrients

30   may stimulate phytoplankton growth, biological activity and then production of abundant fresh

31   autochthonous DOM in the SML. Our results revealed a new enrichment model and the more

32   autochthonous properties of DOM in the SML than the SSW for exploring the oceanic air-sea layer

33   environment.

35   **Keywords:** Sea-surface microlayer; Dissolved organic matter; Photochemical degradation;

36   Enrichment processes; Eastern marginal seas of China

37   **1 Introduction**

38   The sea-surface microlayer (SML) is the boundary interface between the atmosphere and the

39   ocean, which covers about 70% of the Earth's surface. SML is physicochemically distinct from

40   subsurface water (SSW, depth 3 ~ 5 m) and is characteristically enriched with phytoneuston,

41   chlorophyll, particulate carbon, dissolved organic matter (Hardy 1982; Hardy and Apts, 1989), and

42   biogenic organic compounds, such as lipids, proteins, and polysaccharides ((Liss and Duce, 1997; Liss

43   and Duce, 2005). With a total thickness ranging between 1 μm and 1000 μm, the SML remains present

44   in wind speeds of up to 13 m s^{-1} (Sabbaghzadeh et al., 2017). A variety of processes contribute to the

45   formation of the SML in aquatic systems, these include but are not limited to, scavenging by rising

46   bubbles, atmospheric deposition, dissolved organic matter (DOM) photochemical degradation and

47   transformation, secretion, and biodegradation by organisms living within the microlayer (Neuston),

48   and migration of motile organisms into the SML (Aller et al., 2005; Wotton and Preston, 2005). The

49   SML is a very dynamic interface (Cunliffe et al., 2013), the impact of changes in UV radiation on

50   air-sea fluxes in the SML of important trace gases will need to be assessed. In addition, another

51   uncertainty is whether photochemical reactions on the SML affect the flux of volatile species at the

52   air-sea interface (Blough, 1997). Therefore, the role of the microlayer in oceanic emissions is not well

53   understood and fundamental advance in understanding its properties are needed.

54   The processes leading to the enrichment of DOM in the SML are not solely controlled by changes

55   in the DOM concentration at the sea surface microlayer, but are more complex (Mustaffa et al., 2018).

56   Because of its unique position at the air-sea interface, the biological and photochemical reactions of

57   DOM in the SML could strongly impact the biogeochemical cycling of biologically important

58   elements, for example, via the conversion of DOM into volatile species such as carbonyl sulfide

59   (OCS), which influence the atmospheric chemistry and climate (Mopper et al., 2002). Air-sea gas

60   exchanges of trace gases (e.g., CO, OCS, dimethylsulfide (DMS), and alkyl nitrates gases) can also be

61   greatly influenced by biological and photochemical reactions at the sea surface (Blough, 1997).

62   Optical measurements of absorbance and fluorescence have been applied to track DOM

63   variability in aquatic ecosystems (McKnight et al., 2001; Zepp et al., 2004; Coble, 2007). The fraction

64   of DOM that absorbs light in the ultraviolet and visible ranges of the electromagnetic spectrum and the

65   fraction that exhibits a blue fluorescence are known as chromophoric DOM (CDOM) and fluorescence

66   DOM (FDOM), respectively, and their relative compositions can provide information differentiating

67   between autochthonous and allochthonous sources (Coble, 1996; McKnight et al., 2001; Stedmon et

68   al., 2007). Photolysis of DOM promotes the formation of low-molecular-weight compounds,

69   increasing the bioavailability of biologically refractory materials and facilitating carbon uptake by

70   microbes (Kieber et al., 1989). Indices based on optical measurements of absorbance and fluorescence

71   are commonly used to track DOM composition and infer DOM processing due to their low analytical

72   cost and high throughput relative to molecular level analyses (Coble, 2007; Fellman et al., 2010;

73   Gabor et al., 2014). Recent studies have mainly focused on using the characteristics of CDOM as

74   indicators of the sources and degradation states of DOM (Massicotte et al., 2017) in the SSW, and its

75   vertical distribution in estuaries and open oceans (Yamashita et al., 2017; Margolin et al., 2018). In

76   addition, Mustaffa et al. (2018 and 2017) observed that FDOM enrichment in the SML in the coastal

77   regions and open Atlantic Ocean, and FDOM is frequently enriched during upwelling events in the

78   Baltic Sea.

79   Even though there are many studies that have documented the enrichment in DOM (e.g. amino

80 acids; carbohydrates) and inorganic nutrients in the SML relative to the SSW (Orellana et al., 2011;

81 Chen et al., 2016), the differences in organic matter composition between the SML and SSW, the

82 different enrichment factors of DOM in the SML between the coastal regions and the off-shore regions,

83 and how do photochemical degradation activities regulate DOM concentration in the SML need more

84 thorough discussion. Here, we investigated the concentration and composition of DOM in the SML

85 relative to the SSW and the responses of DOM to photoexposure. We hypothesized that the

86 photochemical reactions and enrichment processes could influence the composition difference of

87 DOM between the SML and the SSW, and greater solar exposure in the SML than in the SSW would

88 enhance the mineralization of DOM. To test these hypotheses, our study was designed to answer the

89 questions: (1) What is the differences in optical characterization of DOM between the SML and the

90 SSW? (2) Are the enrichment factors (EFs) of DOM the same between the coastal regions and

91 off-shore regions? (3) How will photochemical degradation processes affect DOM composition in the

92 SML and the SSW? We, therefore, compared the optical properties of DOM between the SSW and the

93 SML, and EFs of CDOM, FDOM components, dissolved organic carbon (DOC), chlorophyll-a (Chl-a),

94 nutrients, and bacterial abundance from the coastal waters to open ocean in the eastern marginal seas

95 of China (including the East China Sea (ECS) and the Yellow Sea (YS)) during spring of 2017 and

96 2019, summer of 2018, and winter of 2019; discuss how the composition of accumulated DOM was

97 affected by environmental conditions (wind speed and salinity) within the SML; and conducted

98 photoexposure experiments to compare photochemical degradation processes of DOM between the

99 SML and the SSW.

100

101 **2 Materials and methods**

102 *2.1* Study Area

103   Four cruises were conducted during the four seasons, specifically, from: 27 March to 15 April

104 2017 (R/V "*Dong Fang Hong 2*"), 26 June to 19 July 2018 (R/V "*Dong Fang Hong 2*"), March 2019

105 (R/V "*Zheyu No. 2*"), and 28 December 2019 to 16 January 2020 (R/V "*Dong Fang Hong 3*"). The

106 station locations are shown in Fig. 1. In spring, summer, and winter, SML samples were collected in

107 the YS and the ECS, which are shallow seas located almost entirely on the continental shelf in the

108 western Pacific Ocean where there is strong interaction between land and sea.
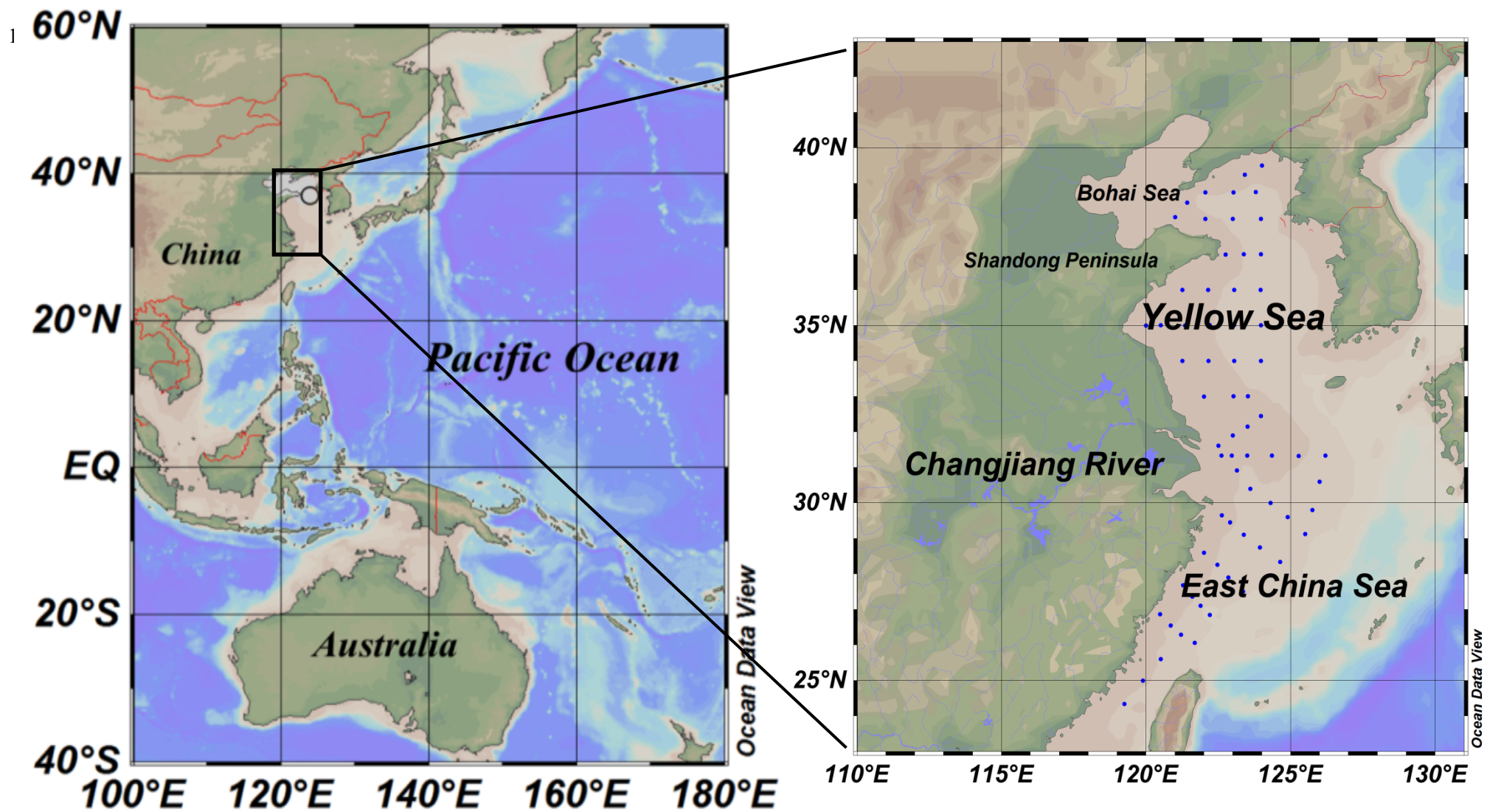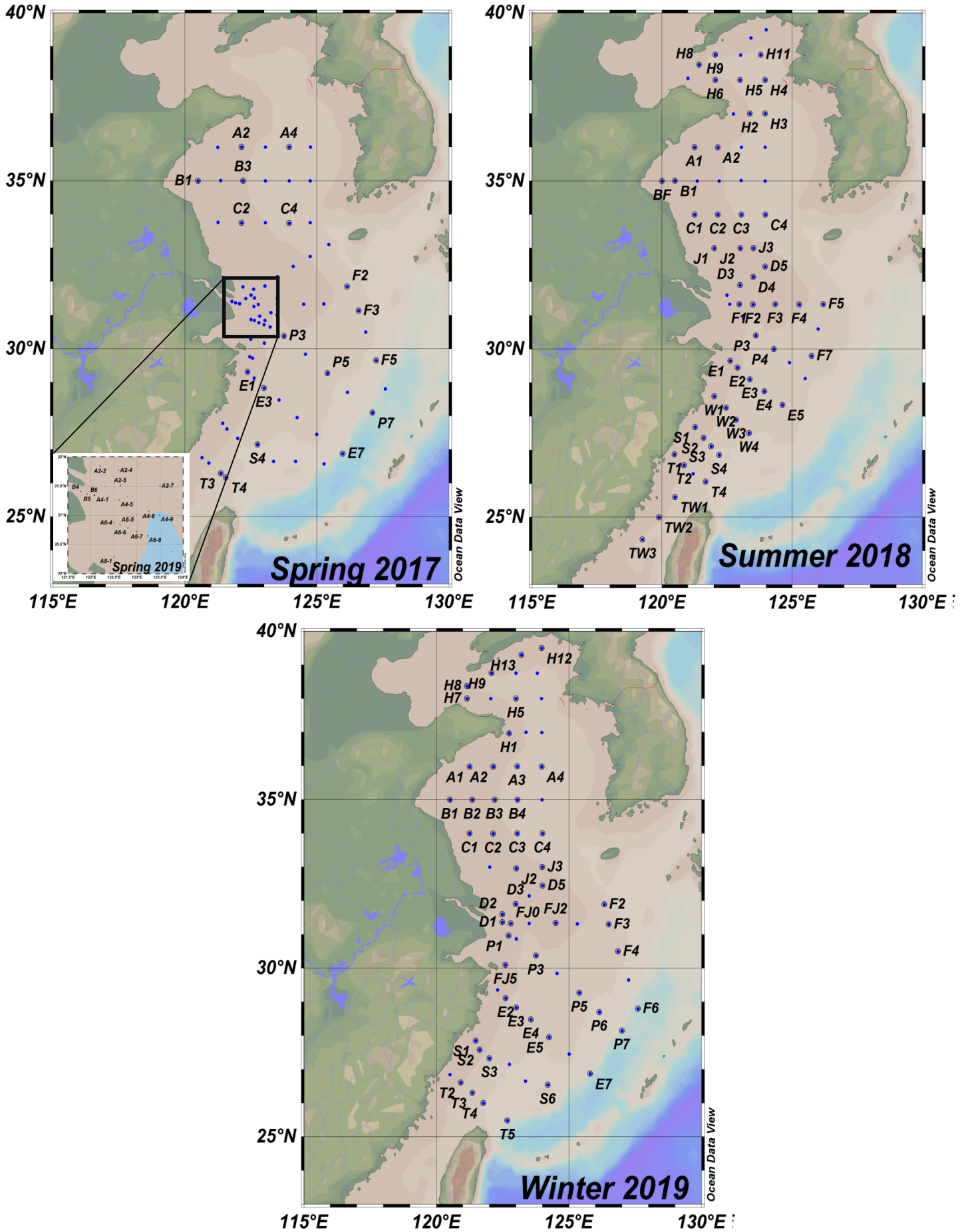
Fig. 1 Map of sampling stations.

112 *2.2 Sampling*

113   We collected 220 paired SML and SSW water samples. SSW samples were collected at 2–5 m

114 depth using 24 × 10-L Niskin bottles mounted on a rosette equipped with a

115 conductivity-temperature-depth (CTD) profiler. The SML samples were collected using the screen

116 sampling technique (Chen et al., 2016; Garrett, 1965) and were taken directly from the ship's bow

117 when conditions were calm. A screen sampler with a 1.6 mm mesh of stainless steel wire on a 40 cm ×

118 40 cm stainless steel frame was used. The SML samples were collected in 500 mL brown sample

119 bottles. The screen was held level and dipped into the sea surface, moved laterally in order to sample

120 from an undisturbed film, and then withdrawn slowly from the surface. Repeated dipping was

121 conducted until the desired volume was collected (11 times, 600 ml; the thickness of the SML sample

122 is nearly 300 ~ 1000 um). The screen method is often applied during field studies because of its

123 relatively short sampling time and large sample volume compared to other techniques (Momzikoff et

124 al., 2004; Chen et al., 2016). Immediately after collection, samples were filtered using 0.7 μm glass

125 fiber filters (GF/F, Whatmann) and the filtrates were transferred to 60 mL and 40 mL brown glass

126 bottles (pre-cleaned and pre-combusted) for later CDOM and DOC analyses. All samples were frozen

127 (-20°C) and protected from light, and upon arriving at the land laboratory, were analyzed as soon as

128 possible. Sea surface temperature and salinity were obtained from a Seabird 911 CTD Rosette.

129 Meteorological data (e.g., wind speed and air temperature) were recorded simultaneously by a

130 ship-borne weather instrument (Li et al., 2019).

131 *2.3 Photoexposure experiment*

132   SSW and SML water samples were collected in July 2018 at stations A3, BF, and H10 as well as

133 D2 and F6 located in the YS and the ECS, respectively. Samples (SSW: 2L; SML: 500 mL) were

134   immediately passed through 0.22 μm PES filters (Pall Corp. Port Washington, NY, USA) to remove

135   the majority of bacteria, placed in acid-washed and pre-combusted brown glass bottles and stored at

136   4°C. Similarly, filtered samples from each site were placed in five 80 mL optically transparent quartz

137   tubes (acid-washed and pre-combusted) and sealed without headspace or air bubbles to measure the

138   effect of light exposure. The quartz tubes were positioned on their sides under the irradiation source to

139   maximize the exposure of the sample; the water depth in each tube was 5 cm (i.e. the diameter of the

140   tube). Both sets (SML and SSW) were irradiated for 6, 12, 24, 50, and 88 h (25°C) in a GLZ-C

141   Quantum Sensor (Top Cloud-Agri Instrument, Zhejiang, China) solar simulator. All samples for DOC

142   concentration measurements were acidified to approximately pH 2.0 with high purity HCl and

143   analyzed within 7 d, and absorbance spectra and fluorescence excitation emission matrices (EEMs)

144   were run on non-acidified samples within 3 d of sampling (4°C and dark).

145   *2.4 Analytical measurements*

146   *Determination of the CDOM absorption coefficient*

147   Absorption spectra were determined using a UV-visible spectrophotometer (UV-2550 bi-channel;

148   Shimadzu, Tokyo, Japan) equipped with two 10 cm path-length quartz cuvettes. Sample absorbance

149   was automatically corrected for the absorbance of Milli-Q water. Absorbance scans ranged from 200 to

150   800 nm, with a spectral resolution of 1 nm. The absorption coefficient of CDOM was calculated

151   according to equation (1):

152    $$a(\gamma) = 2.303A(\gamma)/l \qquad (1)$$

153   where, $A(\lambda)$ is the absorbance at wavelength λ; and r is the path length of the quartz cuvette in meters.

154   The spectral slope of the CDOM absorption curve (S) was calculated according to a non-linear

155   regression over the 275–295 nm and 350–400 nm wavelength range, according to:

156    $$a(\lambda) = a(\lambda_0)\exp[S(\lambda_0-\lambda)]+K \qquad (2)$$

157   where, $\alpha(\lambda)$ is the absorption coefficient at wavelength λ; $\alpha(\lambda_0)$ is the absorption at the reference

158   wavelength λ_0 of 440 nm; S is the spectral slope; and K is a background parameter that accounts for

159   baseline shifts or attenuation due to factors other than CDOM. S was measured in the wavelength

160   ranges of 275–295 nm ($S_{275-295}$, nm^{-1}) and 350–400 nm ($S_{350-400}$, nm^{-1}). $S_{275-295}$ is used to characterize

161   DOM, with high values generally indicative of low-molecular-weight DOM that are linked to

162   photochemical modification (Helms et al., 2008; Ortega-Retuerta et al., 2009). The spectral slope ratio

163   (S_R) was defined as the ratio of the two spectral slopes, $S_{275-295}$ to $S_{350-400}$. S_R is also a sensitive

164   indicator of photochemically induced changes in the molecular weight within the CDOM pool, with

165   increases in S_R suggesting stronger photochemical degradation (Helms et al., 2008; Ortega-Retuerta et

166   al., 2009). We used the absorption coefficient at 254 nm (a(254)) to determine the concentration and

167   distribution of CDOM in the SML from the eastern marginal seas of China. The specific UV

168   absorbance ($SUVA_{254}$) can be used to measure aromaticity (Weishaar et al., 2003) and molecular

169   weight (Chowdhury, 2013) of DOM, with higher values generally indicative of higher aromaticity.

170     $SUVA_{254}$ is calculated as dividing the absorbance at 254 nm by DOC.

171   *EEMs and determination of the CDOM fluorescence index*

172   EEMs were obtained using a F-4500 fluorescence spectrophotometer with a 1 cm quartz cuvette

173   (Shimadzu) (Hoge et al., 1993). The emission spectra were scanned every 5 nm from 250 nm to 550

174   nm, and at the excitation wavelengths between 200–400 nm at 5 nm intervals, with 5 nm slit widths

175   for the excitation and emission modes. The FL Toolbox, which was developed by Wade Sheldon

176   (University of Georgia) for MATLAB, was used to remove the Rayleigh and Raman scattering peaks

177   using the Delaunay triangulation method (Zepp et al., 2004). The fluorescence intensities of the

178   samples were corrected with Milli-Q water blank EEMs and then normalized to the water Raman

179   integrated area maximum fluorescence intensities (Ex/Em = 350 nm/365–430 nm, 5 nm bandpass)

180   (Coble et al., 1998; Singh et al., 2010). Raman units (RU) (Stedmon et al., 2007; Singh et al., 2010)

181   were used as the units for the Raman peak areas of water when the excitation wavelength of 350 nm

182   was used for correction. EEMs were modeled using PARAFAC in MATLAB 7.5 with the DOMFluor

183   toolbox (Stedmon and Bro, 2008).

$$X_{ijk} = \sum_{n=1}^{F} a_{in}\, b_{jn} c_{kn} + \varepsilon_{ijk}$$

184   (3)

185   where X_{ijk} is the fluorescence intensity of the ith sample at the kth excitation and jth emission

186   wavelengths; a_{in} is directly proportional to the concentration (scores) of the nth fluorophore in the ith

187   sample; b_{jh} and c_{kn} are the estimates of the emission and excitation spectra (loadings) of the nth

188   fluorophore at wavelengths j and k, respectively; F is the number of components (fluorophores); and

189   ε_{ijk} represents the unexplained variability of the model (Singh et al., 2010). Split-half analysis

190   validation was used to determine the number of fluorescent components. The fluorescence intensity of

191   each fluorescent component was evaluated (Fig. S2, Supporting Information, Table 1).

192   *Determination of DOC, chlorophyll-a, heterotrophic bacterial abundance, dissolved oxygen, and*

193   *other parameters*

194   Concentrations of DOC were determined using the Shimadzu TOC-V$_{CPH}$ total organic carbon analyzer

195   with an injection volume of 80 μL. The accuracy of the test was ensured by measuring a deep seawater

196   reference (Hansell Laboratory, University of Miami) every 10 samples. Two forms of reference water

197   have been developed for DOC analysis. Deep-ocean water, collected at 2600 m in the Sargasso Sea

198   and containing biologically refractory DOC, as well as low carbon water for testing instrument blanks

199   are available to the U.S. and international communities of aquatic chemists (Hansell, 2013). The Chl-*a*

200   concentration was determined by a fluorescence spectrophotometer (7200-000, Turner Designs, CA)

201   after extraction in 90% acetone based on the procedure of Parsons et al. (1984). DO was determined

202   by iodination using the Winkler titration method (Carpenter, 1964), the endpoint was determined using

203   starch as a visual indicator. Salinity and temperature data were collected in situ by a

204   conductivity-temperature-depth sensor. All phytoplankton samples were enumerated in triplicate

205   according to Specification for Oceanographic Survey (State Bureau of Technical Supervision Bureau,

206   1992). Nutrient species concentrations were determined using an automatic analyzer (QuAAtro, Seal

207   Analytical, Germany) (Grasshoff et al., 2007). All phytoplankton samples were enumerated in

208   triplicate according to Specification for Oceanographic Survey (State Bureau of Technical Supervision

209   Bureau, 1992). Heterotrophic bacterial abundance was measured by flow cytometry (Beckman Coulter

210   FC500-MPL) as described by Marie et al. (1997).

211

The enrichment factor (EF) in the SML is defined as follows

$$EF = C_M / C_S \tag{4}$$

215

where C_M is the concentration of any substance in the SML; and C_S is its concentration in the SSW. If the EF of a substance is greater than 1.0, that substance is considered enriched, if it is less than 1.0, it is considered depleted (Chen et al., 2016).

2.5 Statistical analyses

The correlation coefficient (*R*) and probability (*P*) values were used to evaluate the goodness-of-fit. The correlation matrix, analysis of variance, and principal components analysis were conducted with SPSS version 18.0 (SPSS Inc., Chicago, IL, USA) to determine the possible relationships between the DOM parameters and environmental factors. A *P*-value $\leq$ 0.05 was considered significant. Regression analyses between the optical parameters of DOM and several biogeochemical parameters in the SSW and the SML samples were performed in the Table S1 and the Table S2, respectively.

3. Results and discussion

3.1 Distribution and chemical characterization of DOM in the SSW of the eastern marginal seas of China

The surface distributions of salinity, temperature, CDOM, DOC, Chl-*a*, and several optical parameters in the study area during spring, summer and winter are shown in Fig. S3 (SSW)-S4 (SML) (Supporting Information). There was a strong south-to-north temperature gradient, with warmer waters

233   in the ECS and cooler waters in the YS. Lower salinities were observed in the Changjiang Estuary and

234   coastal waters. The lowest mean wind speed was observed in the summer of 2018 (Table 2). In spring

235   and summer, the bacterial abundances were lower in the YS (spring mean concentration: 2.26×10^8

236   cells/L; summer mean concentration: 3.79×10^8 cells/L) than in the ECS (spring mean: 2.98×10^8

237   cells/L; summer mean: 7.64×10^8 cells/L), indicating that the warmer southern ECS had stronger

238   biological activity in the SSW.

239   The a(254) value ranged from 1.08 to 19.28 m^{-1} in the SML and from 0.82 to 14.23 m^{-1} in the

240   SSW during these three seasons. a(254) values in the Changjiang Estuary (spring: station D1 (4.13

241   m^{-1}); summer: station D2 (3.98 m^{-1}); winter: station D1 (3.14 m^{-1})) and the northern YS (spring: station

242   A2 (4.26 m^{-1}); summer: station H11 (5.37 m^{-1}); winter: station H12 (5.95 m^{-1})) were generally higher

243   than other stations. CDOM absorption values and DOC concentrations were decreased from the

244   inshore to the offshore stations (Fig. S3 c)-d)). There were significantly negative linear correlations

245   between salinity and a(254) in all cruises in the SSW ($p < 0.01$, Fig. 3), especially in the ECS,

246   implying that freshwater run-off and seawater mixing played a more important role in determining

247   CDOM distributions in the SSW. The strongest negative linear relationship observed between salinity

248   and a(254) was observed in winter when the influence of terrestrial input in this study region was

249   maximal. In addition, $SUVA_{254}$ ranged from 0.51 to 8.39 L mg C^{-1} m^{-1} in the SML. In comparison with

250   the SML, the SSW exhibited lower variability in $SUVA_{254}$ values from 0.63 to 5.39 L mg C^{-1} m^{-1}, with

251   higher values at the northern YS stations and Changjiang Estuary coastal stations (Fig. S3k)).

252   According to the $SUVA_{254}$ trends observed by Massicotte et al. (2017), the DOM composition we

253   observed in the SSW of the Changjiang Estuary ecosystem were more similar to the DOM measured in

254   freshwater ecosystems than in the ocean. $SUVA_{254}$ underwent a sharp decrease from the Changjiang

255   Estuary ecosystem to the southeastern ECS, suggesting that aromatic and/or highly conjugated DOM

256   moieties were degraded along the aquatic continuum from the Changjiang Estuary to the open ocean.

257   Higher $S_{275-295}$ values were also observed in some off-shore stations (Fig. S4i)). These comparisons

258   showed that the DOM pools of the Changjiang Estuary contained molecules that were more

259   HMW-DOM and contained more aromatic compounds, CDOM in the SSW of the southeastern ECS,

260   which was derived predominantly from an autochthonous origin (phytoplankton production and

261   bacterial activity), clearly showed the presence of organic matter freshly released into sea (Yang et al.,

262   2020). The detail of mixing behavior, biological and photolytic degradation of dissolved organic

263   matter in the East China Sea and the Yellow Sea were discussed in our previous paper (Yang et al.,

264   2020).

265

266   *3.2 Fluorescence signature and factors controlling the composition of FDOM components in the SSW*

267   *and the SML*

268   FDOM properties can be used as the sensitive indicator of DOM processing and water mass. Four

269   fluorescent components were identified by PARAFAC analysis with the DOM Fluor toolbox in

270   MATLAB 7.5 (Stedmon and Bro, 2008), hereafter named C1, C2, C3, and C4 (Fig. S2). The

271   humic-like C1 and C3 were categorized as two traditional types of humic-like fluorescent components

272   (Coble 1996). Component 1 had primary fluorescence excitation and emission peaks at 345 nm and

273   455 nm, respectively, which was similar to terrestrial humic-like fluorophores in the visible region

274   (peak C) (Osburn et al., 2012). Relative to C1, the fluorescence of C3 was blue-shifted and had

275   fluorescence peaks at 385 nm emission and 315 nm excitation. The microbial humic-like component

276   had a relatively shorter emission peak wavelength compared to the terrestrial humic-like PARAFAC

277   components previously identified in the open ocean (Catala et al., 2015). C2 exhibited Ex/Em maxima

278   at 255 nm/310 (375) nm, which could be considered tyrosine-like fluorescence (Stedmon et al., 2003)

279   and attributed to autochthonous and/or microbial FDOM. C4 had an excitation range of 280 nm with

280   an emission peak at 335 nm, which corresponded to peak T of the amino-acid-like fluorescence of

281   tryptophan, likely derived from in situ primary autochthonous substances and other fresh biological

282   sources (Coble, 1996). The tryptophan-like C4 and the humic-like C1 and C3 in the SSW were all

283   negatively correlated with salinity ($P < 0.01$, Table S1), but increased with the increasing DO level.

284   These suggested that water mixing and microbial activity were important factors in determining

285   geographical distributions of FDOM in the SSW (Breitburg, et al., 2018; Yamashita et al., 2017;

286   Galgani and Engel, 2016). Moreover, the geographical distribution of humic-like C1 and protein-like

287   components were more similar to that of the Chl-a concentration in the SML (Fig. 4 a, b, d). Such

288   relationships suggested that the production of protein-like and humic-like FDOM with phytoplankton

289   production and decay in the SML.

290   FDOM enrichment in the SML of all stations ranged between 0.5 and 11 (n = 225) and FDOM

291   was more frequently enriched (C1: 89.6%; C2: 73.2%; C3: 91.8%; C4: 93.4% of all samples) than

292   CDOM. The fluorescence intensity of the components in the SML samples decreased in the following

293   order: tryptophan-like > tyrosine-like > terrestrial humic-like > marine humic-like; whereas those in

294   the SSW samples decreased in the order: tyrosine-like > tryptophan-like > marine humic-like >

295   terrestrial humic-like. The tryptophan-like component (C4) was mostly enriched in the SML samples

296   with a median EF = 2.2 and a range from 0.2 and 8.0. The EF of C4 was clearly higher than other

297   components in all seasons (Fig. 6b)), especially in summer, and the FDOM composition in the SML

298   revealed a relatively higher proportion of autochthonous tryptophan-like FDOM than the SSW. It has

299 also been broadly recognized that tryptophan-like C4 in the particulate fraction is related to recent

300 primary production (Brym et al., 2014; Yamashita, 2014) and that phytoplankton excrete

301 tryptophan-like fluorophores (Romare-Castillo et al., 2010). Together, as already emphasized

302 previously, the variation observed for FDOM can be more related to that of Chl-a in the SML, these

303 observations suggested that the DOM enriched in the SML was made up of a relatively higher

304 proportion of marine autochthonous DOM than the SSW.

305

306 *3.3 DOM and biogenic molecules accumulation in the SML*

307 Up to 88% of our CDOM samples were enriched in the SML, with the median EF for a(254) of

308 1.3, ranging between 0.4 and 6.7. Concentrations of CDOM, FDOM, nutrients, bacterial abundance,

309 and Chl-*a* in the SML were correlated with their respective SSW concentrations (Fig. 5),

310 demonstrating that transport from the SSW to the SML is an important pathway. Furthermore, the

311 relatively higher CDOM absorption enrichment value in the SML were found at longer wavelengths

312 (Fig. 6a)) EF of a(355) > EF of a(254)). Marine DOM usually has higher absorption slope than

313 terrestrial DOM, and the higher slope (no matter it is $S_{320-412}$ or $S_{275-295}$), marine production of DOM

314 had the largest influence on the CDOM absorption properties in the longer wavelength range (Danhiez

315 et al., 2017) ($S_{320-412}$: DOM marine origin VS. $S_{275-295}$: terrestrial DOM).

316 Galgani and Engel (2016) also observed that amino acid-like fluorophores were highly enriched

317 in the SML, not only due to their amphiphilic properties, but also due to their local production in the

318 SML. Therefore, the marine local production might significantly affect the composition of DOM in the

319 SML. Additionally, the nutrients showed significantly higher EFs (NO_3^-: 3.41 ± 6.08, n = 41; NO_2^-:

320 3.57 ± 5.54, n = 52; PO_4^{3-}: 2.13 ± 2.74, n = 68; and SiO_3^{2-}: 6.53 ± 13.67, n = 13) than biological and

321 DOM parameters in the SML. The strong correlation between the SML and SSW concentrations of

322   NO_2^-, NO_3^-, and SiO_3^{2-} (Fig. 5) showed that the similar fundamental drivers are probably at work in

323   both compartments for these nutrients. For example, dissolved substances, particles, and

324   microorganisms were brought to the interface by simple diffusion, rising bubbles (Jarvis, 1967),

325   convection, and upwelling from sediments and subsurface water, and at the same time, the microlayer

326   is also a sink for fallout from the atmosphere (Duce et al., 1976). In addition, we also observed the

327   significant positive relationship between a(254) and Chl-*a* ($R = 0.662$, $P < 0.01$) in the SML during

328   spring, and the positive relationship between the EF of PO_4^{3-} and the EF of Chl-*a* ($R = 0.319$, $P = 0.01$,

329   Table 3). These observations indicated that spatial variation of CDOM concentrations were related to

330   Chl-a in the SML. The enrichment of inorganic nutrients would be an important factor influencing the

331   production and composition of phytoplankton-produced DOM (Carlson and Hansell, 2003) in the

332   SML. Therefore, phytoplankton growth, primary productivity rate, biological activity and marine

333   autochthonous DOM production would all be enhanced by the enriched nutrients in the SML.

334

335

336

337

338

339
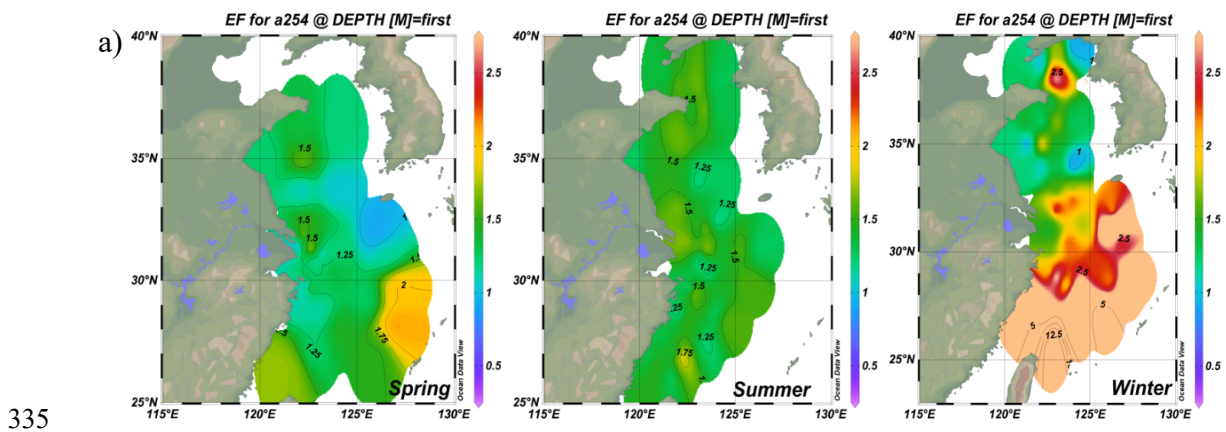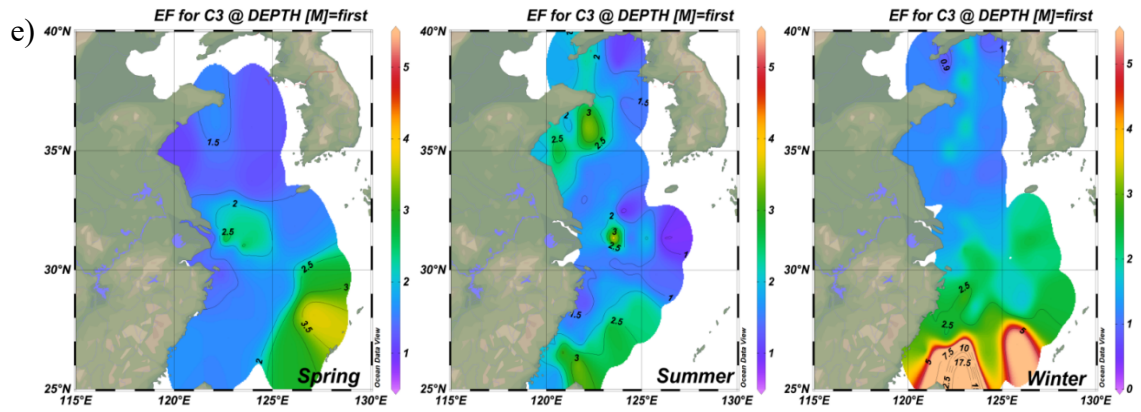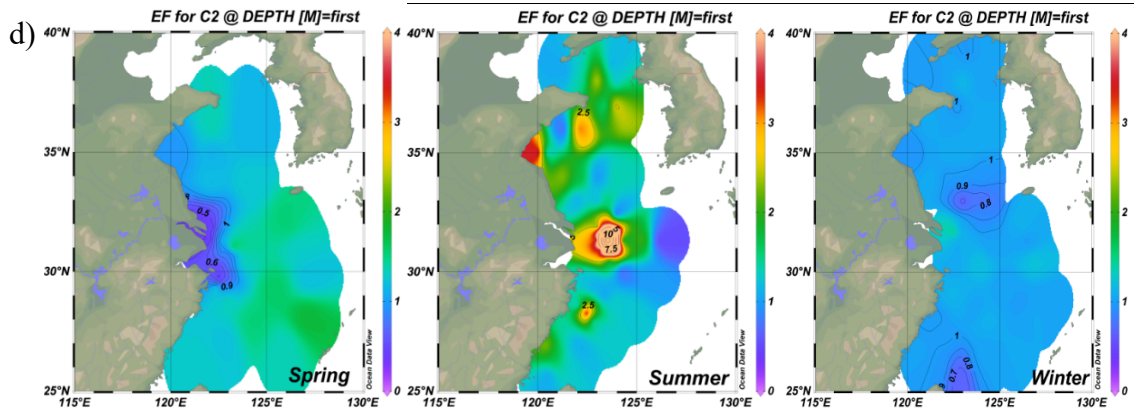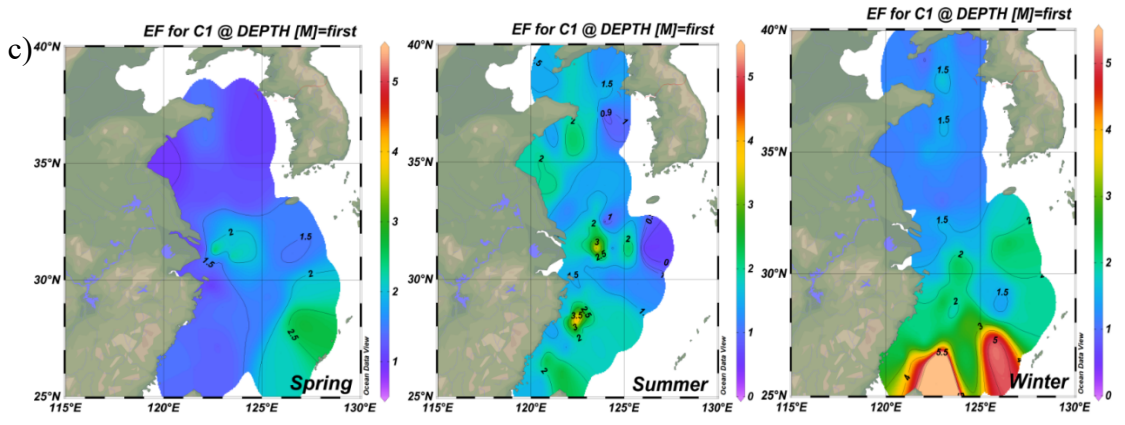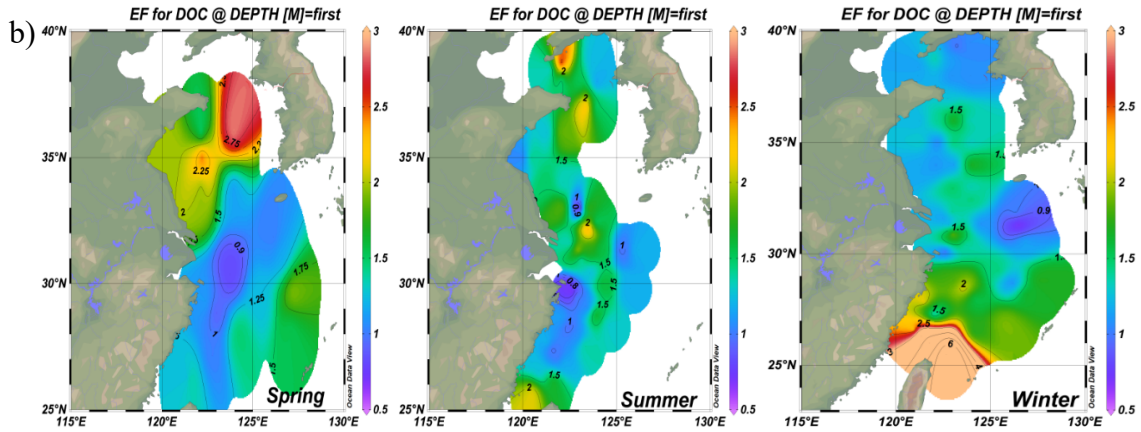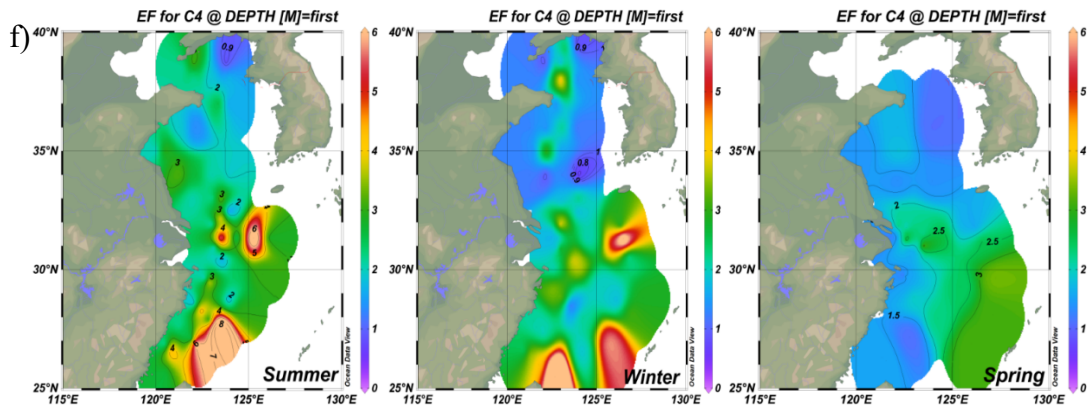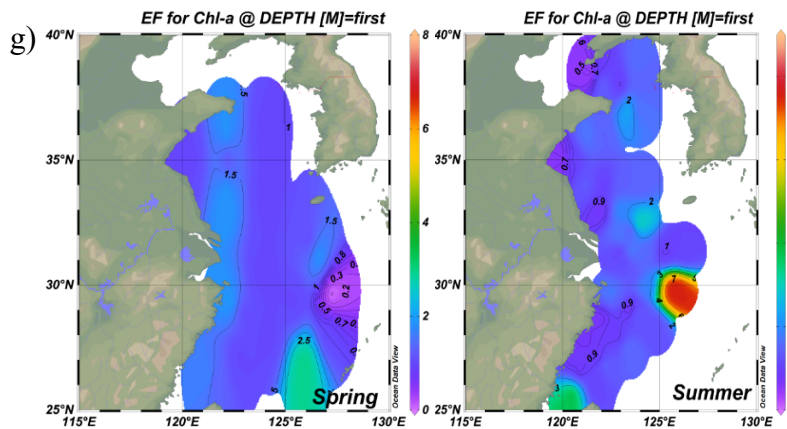
Fig. 2. Distributions of enrichment factors of CDOM, DOC, Chl-*a*, and four fluorescence components in the surface microlayer water during spring, summer, and winter. Increasing DOM yields were significant in coastal regions in all seasons, but the higher enrichment factors (EFs) were more pronounced in off-shore regions.
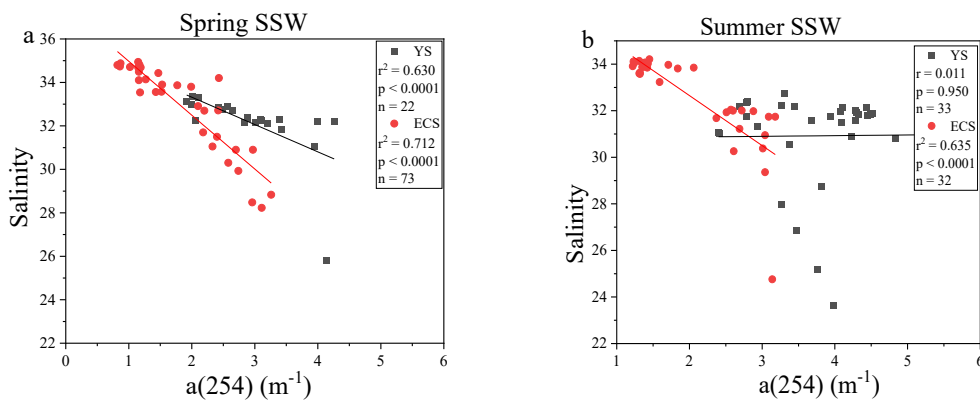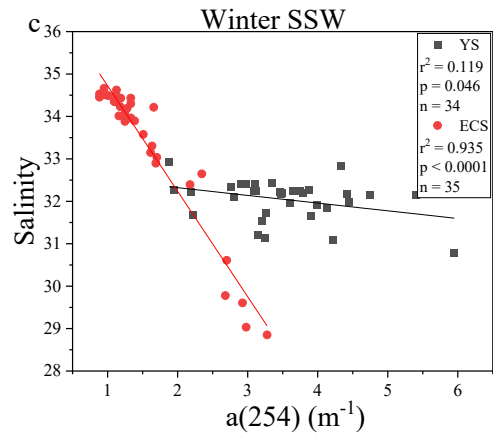
347

348 Fig. 3. Relationships between a(254) and salinity in the subsurface water (SSW) in the East China Sea

349 (ECS) and the Yellow Sea (YS) during spring, summer and winter.

350

351

352

353

354
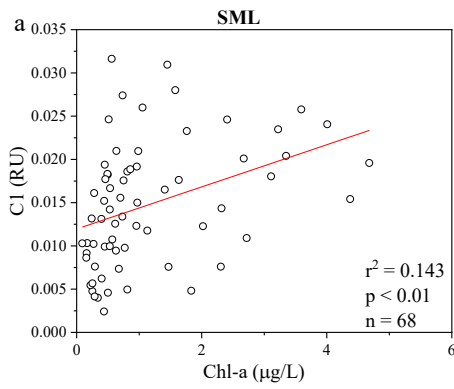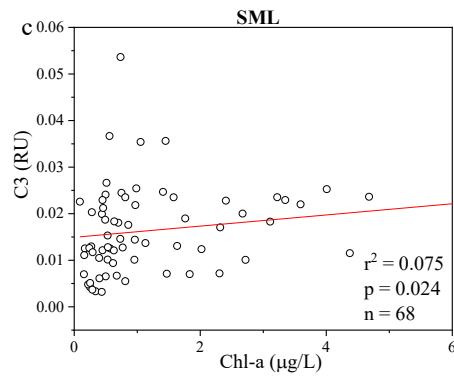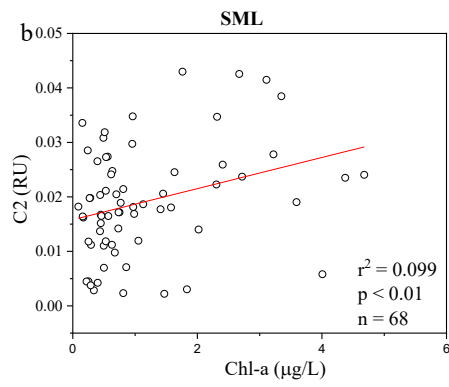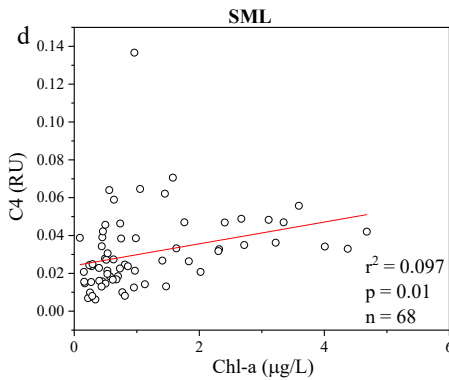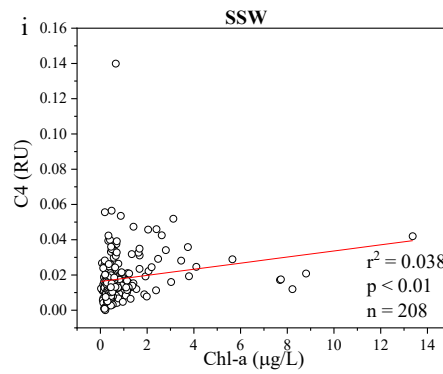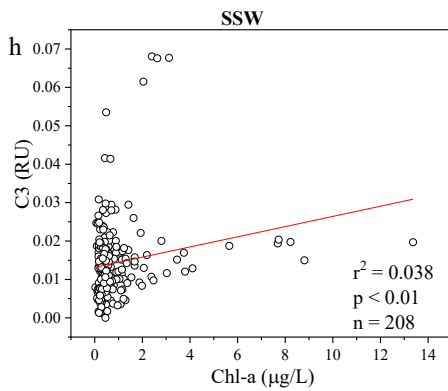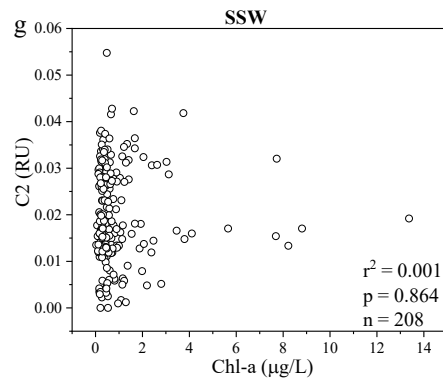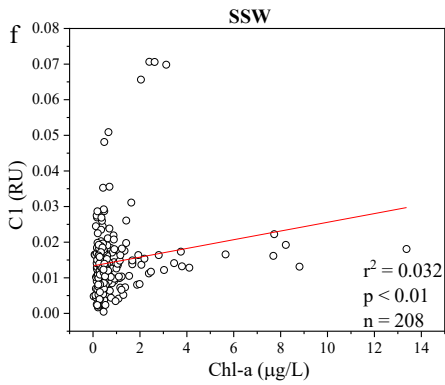
355 Fig. 4. Relationships between a(254), four fluorescence components and Chl-*a* in the sea-surface
356 microlayer (SML) (a-d) and in the SSW (f-i).
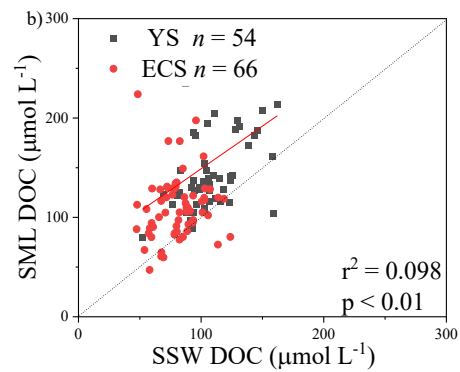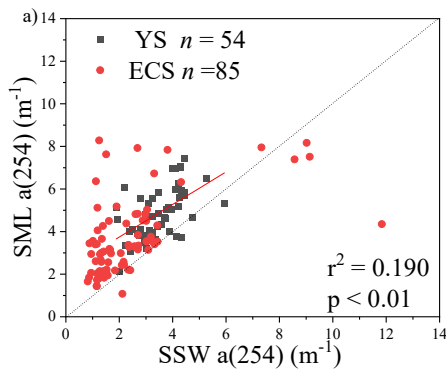
357
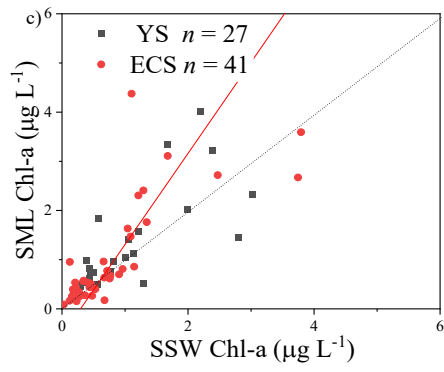
358
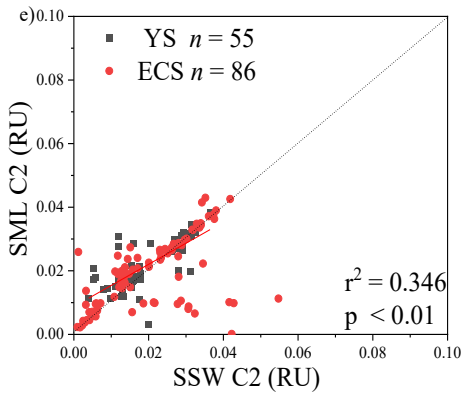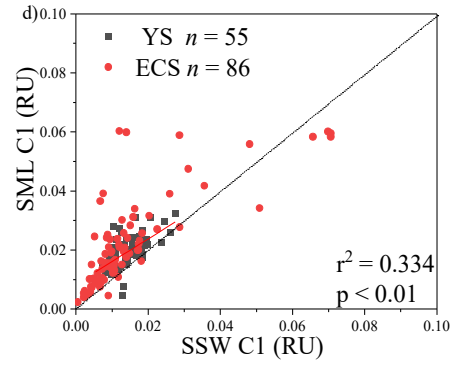
359

360

361

362

363
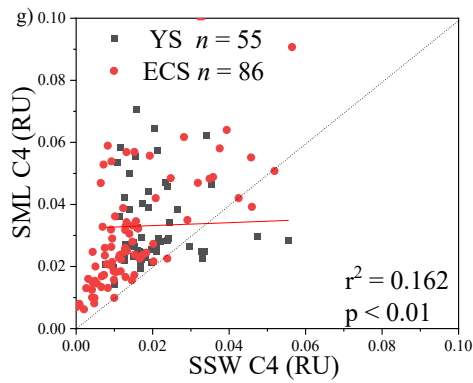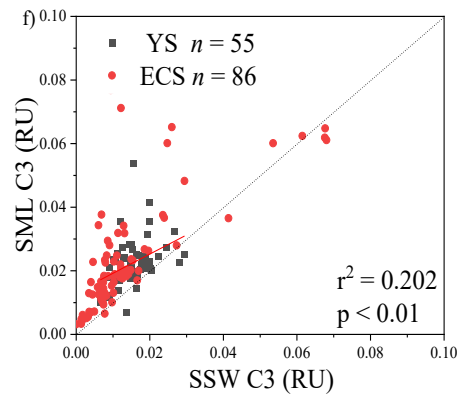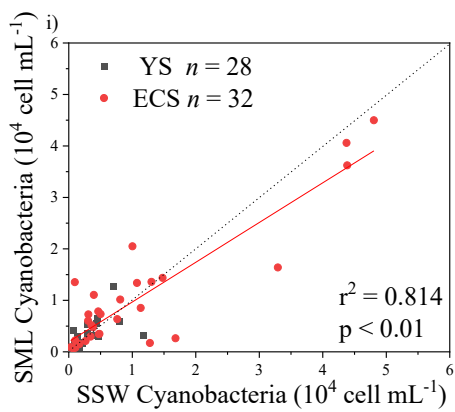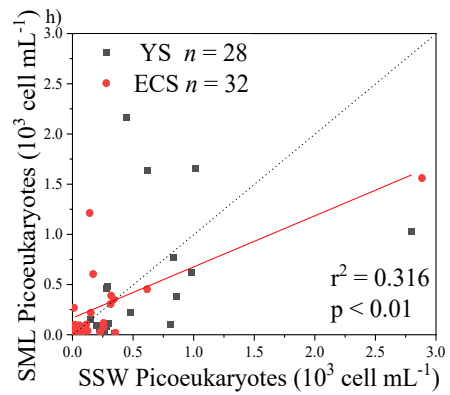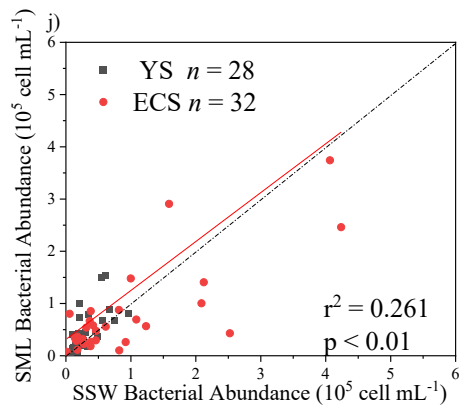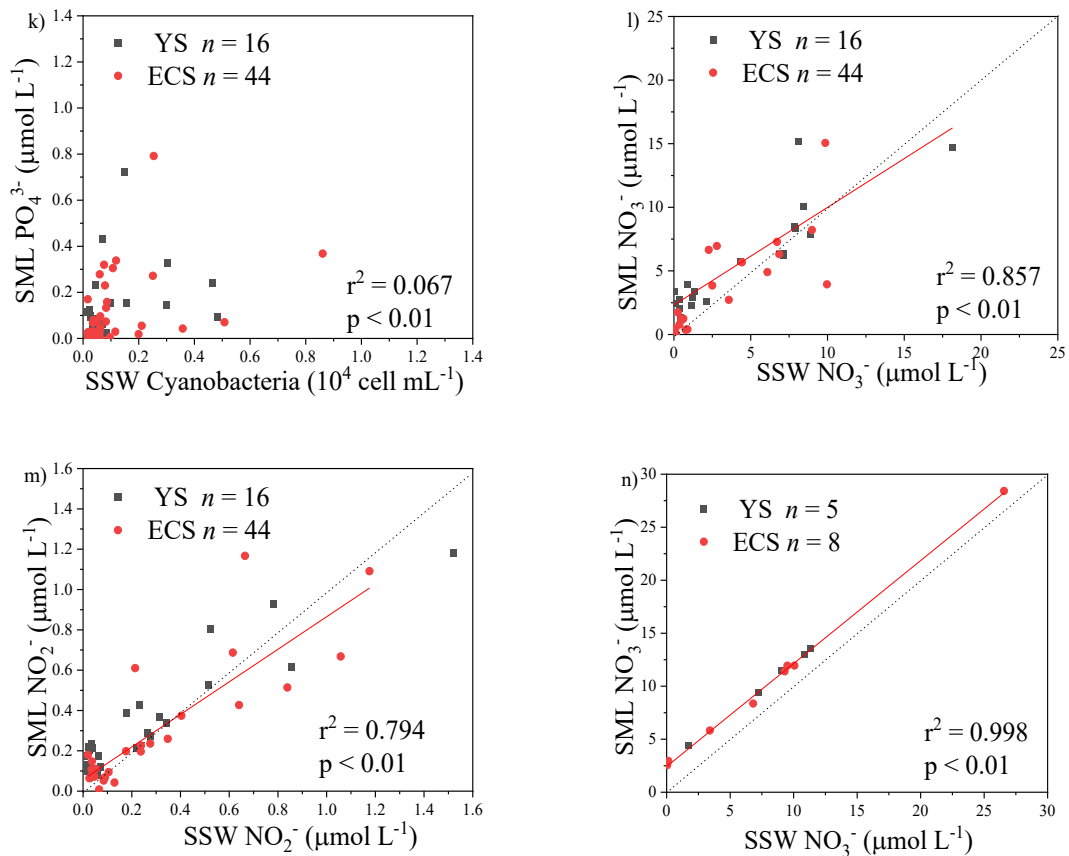
364   Fig. 5. Correlations between the microlayer CDOM, DOC, Chl-*a*, four fluorescence components

365   concentrations, cyanobacteria, phytoplankton biomass, nutrients and bacterial abundance, and their

366   subsurface water concentrations. The dashed lines correspond to the 1:1 lines, and the full lines are the

367   regression models. (All DOM spectroscopic parameters sample were analyzed in spring, summer and

368   winter; Chl-*a* was determined in spring, summer, and summer; cyanobacteria, phytoplankton biomass,

369   nutrients and bacterial abundance were determined in spring and summer.).

370
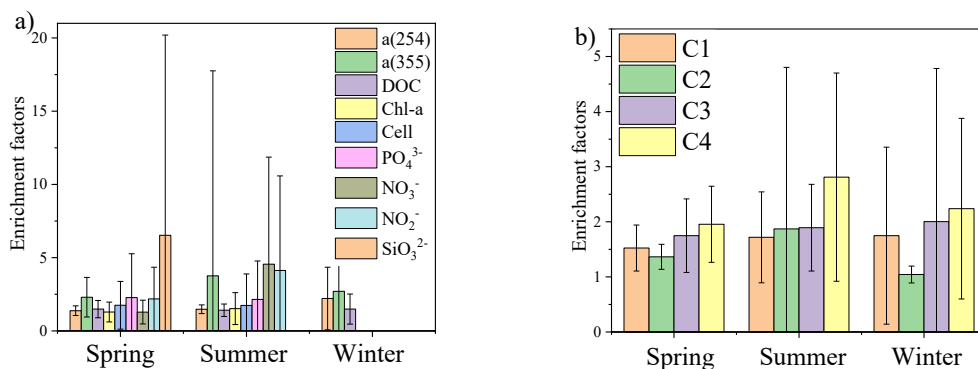
371   Fig. 6. Mean enrichment factor of a_{CDOM} (254 nm and 355 nm), DOC, Chl-*a*, nutrients (PO_4^{3-}; NO_3^-;

372   NO_2^-, SiO_3^{2-}), and four fluorescence components during spring, summer, and winter.

373

374   *3.4 Wind speed influencing the enrichment of DOM optical properties*

375   The wind speeds during our observations ranged from 0.2 to 14.9 m s^{-1}. We divided them into

376   three different wind regimes: low (0.0–2.0 m s^{-1}), moderate (2.0–10.0 m s^{-1}), and high (10.0–14.9 m

377   s^{-1}). Although the EFs of DOC and Chl-*a* were negatively correlated with wind speed (DOC: $P = 0.002$;

378   Chl-*a*: $P = 0.042$), the EFs of CDOM and FDOM were not. During the low wind regime, no

379   significant relationships were apparent between wind speed and either EFs of CDOM or FDOM,

380   CDOM and FDOM were consistently enriched, with EFs ranging from 1.0 to 2.2, and a mean a(254)

381   EF value of 1.3 (n = 20). However, the EFs during moderate winds had larger variability and ranged

382   from 0.9 to 14.5, with a mean EF value of 1.6 (n = 143), and during high winds they ranged from 0.6

383   to 1.8, with a lower mean EF value of 1.1 (n = 18). In addition, depleted levels of CDOM (EF < 1)

384   occurred at frequencies of 5.6%, 9.1%, and 20.0% during low, moderate, and high wind regimes,

385   respectively. Therefore, although lower wind speeds and ascending bubbles might further promote the

386   transportation of organic materials from the underlying waters, DOM enrichments were still observed

387   at wind speeds up to > 10 m s^{-1}. Reinthaler et al. (2008) also reported that higher enrichment was

388   found at higher wind speeds. During moderate to high wind regimes, breaking waves not only can

389   disrupt the surface film and physically drive DOM back into the bulk water, but also facilitate the

390   formation of the SML as rising bubble plumes transported DOM to the surface, resulting in wider

391   ranges of EFs (Frew et al., 2004). Higher wind speed does enhance mixing (Reinthaler et al., 2008),

392   which can arguably favour transport of nutrients and DOM from the SSW equally (Wurl et al., 2011).

393   Although wind speed appear to play an important role in the enrichment of surface-active DOM, the

394   chemical composition of the SML influence its stability. For example, enrichments of sulphate

395   half-ester groups in the SML (Wurl and Holmes, 2008) could increase stability because these groups

396   can influence the intrinsic viscosity of marine polymers (Nichols et al., 2005) and sulphur-containing

397 algal carbohydrates are less soluble and hydrolysable (Kok et al., 2000). Sampling needs to be

398 performed on the leeward side of the boat with the boat moving into the wind to aboid contamination.

399 Although some disturbance of SML integrity was produced by the ship's movement and potential

400 contamination at high wind speeds and tidal mixing. It has long been known that the SML reforms

401 rapidly following physical disruption (Dragcevic and Pravdic, 1981). Rapid SML recovery occurs

402 because SML organics dispersed by breaking waves readily reabsorb to the surfaces of rising bubbles

403 generated by the same breaking waves (Woolf, 2005). Enrichment processes and biochemical

404 processes of organic substances in the marine environment are all likely to be the more important

405 contributors of DOM to the SML in our study regions.

406 *3.5 Photochemical degradation of DOM in the SSW and the SML*

407  Photobleaching is one of the major mechanisms determining the geographical distributions of

408 chromophoric and fluorescent DOM in the ocean (Helms et al., 2008; Brinkmann et al., 2003; Siegel

409 et al., 2005). The average $SUVA_{254}$ values in SSW were generally higher than those in the SML in our

410 study regions (SSW: 2.45 ± 0.91 L mg-C^{-1} m^{-1} vs. SML: 2.39 ± 1.34 L mg-C^{-1} m^{-1}), and the most

411 obvious distinction happened in summer (Table 2). These indicated that although CDOM

412 concentration in the SSW was lower than that in the SML, CDOM in the SSW has a higher degree of

413 aromaticity compared to the SML. Thus we performed photochemical incubation experiments to

414 confirm whether photochemical reactions influenced the differentiated aromaticity and photo-reactive

415 features of DOM between the SML and the SSW.

416  After 88 h of exposure, the a(254) values were only 49.6%, 45.5%, 42.1%, 41.8% and 37.0% of

417 the initial values at stations A3, BF, D2, F6, and H10 in the SSW, and 72.5%, 42.4%, 42.6%, 49.0%

418 and 44.0% of the initial values at stations A3, BF, D2, F6, and H10 in the SML, respectively. Overall,

419   a(254) and SUVA$_{254}$ decreased by 49.9 ± 12.8% and 43.0 ± 15.5%, respectively, in the SML, and by

420   56.8 ± 4.7% and 56.0 ± 10.2%, respectively in the SSW. Therefore, stimulated solar UV exposure

421   caused a larger decrease in DOM absorbance in the SSW than the SML (Fig. 7). The relatively rapid

422   decrease of SUVA$_{254}$ in the SSW indicated a more rapid conversion of DOM to less humic-type

423   materials than in the SML. Although photodegradation causes CDOM absorption to decrease, DOC is

424   not sensitive to photodegradation in our photodegradation experiments, implying that the light

425   exposure preferentially removed the colored DOM rather than the non-colored DOM (Bittar et al.,

426   2015). All incubation samples were not contaminated, both measurement and analytical errors will let

427   DOC data exceed 100%. Approximately 65% of FDOM was lost during the irradiation experiment,

428   except in the case of the tyrosine-like component 2 from the SML at the station H10, which increased

429   slightly. Photoproduction of tyrosine-like components has been previously reported by Zhu et al.

430   (2017), who suggested that the photochemical degradation of CDOM contributed to the release small

431   amounts of tyrosine-like fluorophores. The tryptophan-like C4, humic-like C1 and C3 were more

432   photodegradated in the SSW than in the SML (Fig. 7c), e), f)). For example, C1, C3 and C4 show a

433   marked decrease in the SSW at the off-shore station F6. Because of the origin of CDOM at the station

434   F6 remote from the direct terrestrial influence, the majority of CDOM at the station F6 was thought to

435   be a by-product of net primary production. The present results showed that a large fraction of the total

436   CDOM in the SSW at the off-shore station F6 is still potentially sensitive to photooxidation. As

437   already referred previously, CDOM in the SSW showed higher SUVA$_{254}$ values, and higher

438   percentages of humic-like DOM than in the SML. Therefore, the photochemically mediated shifts in

439   DOM in the SSW were more pronounced than those in the SML in our incubation experiments, in

440   terms of both absorption and fluorescence values.

441   This heterogeneity in the EFs and photochemical reactivities of FDOM components can be

442   related to the chemical and structural nature, such as molecular weight, aromaticity or humification of

443   FDOM enrichment processes. Hydrophilic, carboxylic acid-bearing DOM moieties are preferentially

444   degraded by simulated sunlight (Brinkmann et al., 2003). The largest fractions of photolabile DOM are

445   made up of aromatic carbon rings or high double bond equivalent molecules (Kujawinski et al., 2004;

446   Gonsior et al., 2009). The humic-like C1 and C3, all of which exhibited significantly positive

447   relationships with $SUVA_{254}$ (< 0.001, Table 1) and shown higher aromaticity, were more prone to

448   photochemical degradation (Fig. 7c), e), and f)). The tyrosine-like C2, as compared to other

449   protein-like compounds, is generally considered more labile and susceptible to bacterial cycling and

450   rapid consumption by microbiota (Medeiros et al., 2015). The SML experiences the most intense solar

451   radiation, especially ultraviolet (UV) light (Obernosterer et al., 2005). Photochemical degradation may,

452   therefore, be a sink for aromaticity fluorescent components in the SML, and be a source for the

453   tyrosine-like C2. In addition, Blough (1997) discovered that photochemical production rates in the

454   SML should lead to the more rapid oxidative turnover of materials at the interface and potentially to

455   reactions and processes not observed in bulk waters. Therefore, differences in $SUVA_{254}$ values and

456   photoreaction behavior between the SSW and the SML may also reflect that DOM in the SML was

457   already photobleached, which resulted in the decrease of DOM aromaticity, CDOM in the SSW

458   appeared to be more susceptible to photochemical degradation than CDOM in the SML. Together,

459   photo-irradiation have the significant influence on the accumulation of protein-like DOM and

460   depletion of aromatic organic compounds in the SML, and organic carbon might have undergone a

461   more rapid cycling in the SML than the SSW.

Fig. 7. Changes in ratios of a(254), DOC, SUVA$_{254}$ and four fluorescence components intensities to initial values for both SML and SSW sample.

3.6 Variations in the enrichment factors of CDOM, DOC, FDOM along the coastal regions to ocean

The concentrations of a(254) and DOC decreased from the coastal regions to the open ocean, and decreased from the northern part of the sampling area (the YS) to the southern part of the sampling area (the ECS) in both the SSW and the SML (Fig. S3 c)-d) and Fig. S4 a)-b)). However, CDOM and FDOM were more frequently enriched in the ECS (CDOM: 93% of all samples; FDOM: 72–94% of all samples) than that in the YS (CDOM: 86% of all samples; FDOM: 70–92% of all samples). The higher EF values for CDOM, FDOM, DOC, Chl-*a*, nutrients, and cell were generally observed in the ECS (Fig. 2). Lower EFs and EFs < 1, which indicate a depletion of CDOM in the SML, were usually observed at short distances from the coast (Fig. 2) with lower salinity. The salinity during our

477   observations ranged from 23.6 to 35.1. Although CDOM and FDOM concentration negatively

478   correlated with salinity, the EFs of CDOM and FDOM were weakly positive related with salinity (Fig.

479   8). The EFs of Chl-*a* and nutrient were also higher in the southeastern ECS (Fig. 2 and Fig. S5), where

480   sufficient light and higher temperature combined to facilitate primary production and higher

481   contributions of autochthonous materials to DOM. DOM in the SSW of the southern ECS was more

482   dominated by marine autochthonous materials in our previous discussion (Yang et al., 2020). The

483   Changjiang River discharges enormous amounts of N and P into the ECS (Liu et al., 2018), but

484   phosphorus is generally the major limiting element for phytoplankton growth in the ECS (Liu et al.,

485   2016). Thus the difference in EFs of CDOM and Chl-a between YS and the ECS, and between the

486   coast and off-shore regions is likely due to the significantly nutrients enrichment in the SML in the

487   off-shore regions. In winter, we observed especially higher EF values for CDOM and FDOM in the

488   southern ECS (Fig. 2a)-f)). With wind from the northwest (Weng et al., 2011), biologically essential

489   trace elements and anthropogenic emissions are carried from the land and can enter the ocean via the

490   SML by wet or dry deposition. The EFs of humic-like C1 and C3 were relatively high in winter (Fig.

491   6b)), probably due to the input from atmospheric deposition during winter, and the relatively low

492   CDOM concentrations in bulk water. Atmospheric deposition of organic carbon and nutrients were

493   found a peak in winter over the coastal ECS (Wang et al., 2019). We suggested that the EFs of CDOM

494   and FDOM increased from the coastal regions to the open ocean, and increased from the YS to the

495   ECS were likely due to the enrichment of enough nutrients in the SML in the open ocean promote

496   phytoplankton biomass and DOM production.

497

498

499
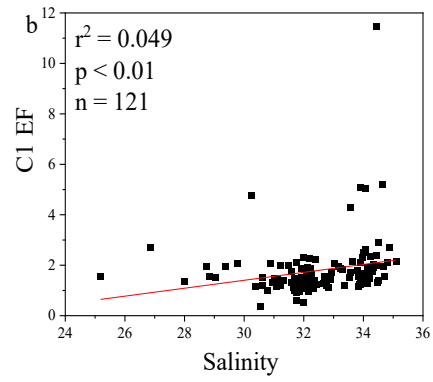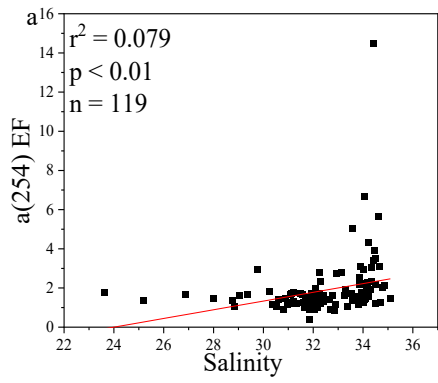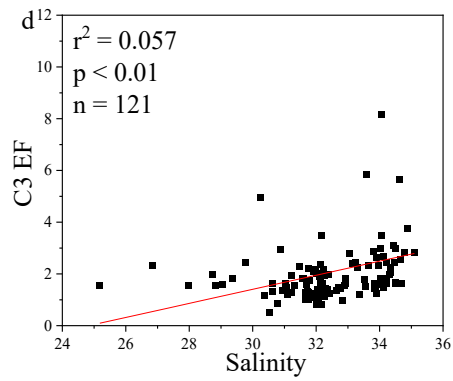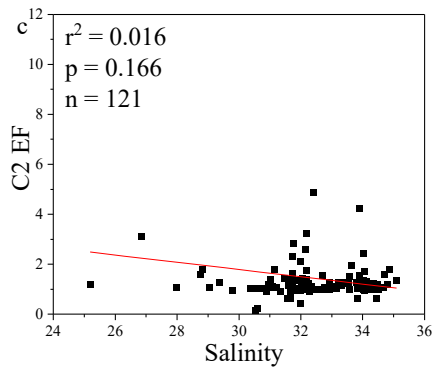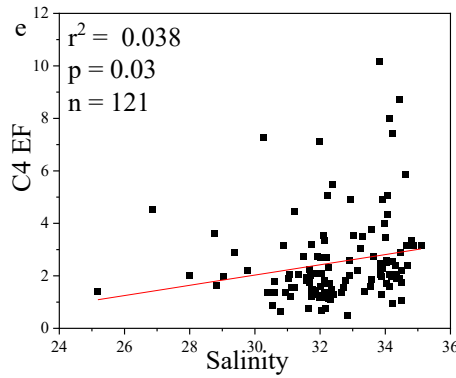
500 Fig. 8. Relationships between salinity and EFs of a(254), Chl-a, DOC, and four fluorescence
501 components.

502   The SML is an aggregate-enriched biofilm environment with distinct microbial communities,

503   where the diversity of microorganisms can differ significantly from those of underlying waters (Liss

504   and Duce, 2005; Cunliffe et al., 2013), the heterotrophic bacterial abundance in the SML was ~ 7.5

505   fold greater than those in the SSW in the ECS during our spring cruise (Sun et al., 2020). Here, EFs

506   showed a greater presence of bacteria and marine protein-like DOM in the SML than that in the SSW,

507   while the protein-like DOM was linked to microbial utilization and degraded faster than the humic-like

508   substances (Yang et al., 2017; Jørgensen et al., 2011). Therefore, compared to coastal waters that have

509   larger terrestrial DOM and nutrients inputs, CDOM shown higher EFs in off-shore regions where

510   DOM in the SSW is mostly of marine autochthonous origin with higher temperatures and stronger

511   biological activity. The significantly higher abundance of cells, phytoplankton, nutrients, and

512   protein-like DOM in the SML supported microbial activities, and further contributing to the local

513   release of marine extracellular DOM directly from microbes in the SML in the off-shore regions.

514   When exposed to higher light intensities (summer), obviously enhance mineralization of DOM in the

515   SML, and relatively less photochemical degradation in SSW could result in lower percentage of

516   aromatic DOM in SML than the SSW. We concluded that SML CDOM dynamics can be expressed as

517   a complex balance among enrichment process, primary production and photochemical destruction.

518   Thus, higher EF of DOM in the SML in off-shore regions are likely supported by a favorable

519   combination of: 1) deposition and accumulation of amphiphilic compounds, 2) importance of bubble

520   for upward transport of DOM and enrichment in SML, and 3) new production of DOM within the

521   SML as a consequence of higher nutrients enrichment and the primary production.

522

523   **4. Conclusions**

524   This study has provided the first data set that considers the distributions of CDOM, FDOM, DOC,

525   Chl-*a*, nutrients, and bacterial abundances in the SML and SSW of the ECS and the YS during spring,

526   summer, and winter. We have observed that the CDOM distribution related variability in primary

527   production in the SML. Furthermore, we have demonstrated that localized and stronger photochemical

528   oxidation may be responsible for the decrease in the aromaticity of the DOM in the SML, due to

529   enhanced transformation or removal of terrestrial DOM, compared with the SSW. We also

530   demonstrated that in off-shore seawaters away from terrigenous influence, the EFs of CDOM, DOC,

531   FDOM and Chl-a in SML tend to be higher in off-shore regions than those in coastal regions, because

532   of the relatively higher enrichment of nutrients which could enhance phytoplankton growth and

533   promoted plant production and DOM production in the SML. Multiple observations of spatial

534   distributions, seasonal variations, chemical compositions, and photochemical reactions of CDOM in

535   the SML have supported the hypothesis that stronger enrichment and photochemical processes occur in

536   the SML in ocean, resulting in relatively accelerated enrichment of more marine local production

537   DOM in the SML than the SSW.

538

539   **Acknowledgements**

540   We thank the captain and crews of the R/V '*Dong Fang Hong 2*', the R/V '*Dong Fang Hong 3*',

541   and the R/V '*Zhe Yu 2*' for their assistance and cooperation during the investigation. We gratefully

542   acknowledge Ya-Hui Gao (Xiamen University), Yu Xin (Ocean University of China), and Xiao-Hua

543   Zhang (Ocean University of China) for providing the Chl-*a*, nutrients, bacterial abundance and

544   picoplankton data, respectively. This work was financially supported by the National Key Research

545   and Development Program (Grant No. 2016YFA0601304), and the National Natural Science

546   Foundation of China (Grant Nos. 41806093 and 491830534).

547

548 **References**

549 Aller, J.Y., Kuznetsova, M., Jahns, C.J., Kemp, P.F.: The sea surface microlayer as a source of viral

550 and bacterial enrichment in marine aerosols. J. Aerosol Sci. 36(5), 801–812.

551 https://doi.org/10.1016/j.jaerosci.2004.10.012. 2005.

552 Bittar, T.B., Vieira, A.A.H., Stubbins, A., Mopper, K.: Competition between photochemical and

553 biological degradation of dissolved organic matter from the cyanobacteria Microcystis aeruginosa.

554 Limnol. Oceanogr. 60(4), 1172–1194. https://doi.org/10.1002/lno.10090. 2015.

555 Breitburg, D., Levin, L.A., Oschlies, A., Grégoire, M., Chavez, F.P., Conley, D.J., Garçon, V., Gilbert,

556 D., Gutiérrez, D., Isensee, K., Jacinto, G.S., Limburg, K.E., Montes, I., Naqvi, S.W.A., Pitcher,

557 G.C., Rabalais, N.N., Roman, M.R., Rose, K.A., Seibel, B.A., Telszewski, M., Yasuhara, M.,

558 Zhang, J.: Declining oxygen in the global ocean and coastal waters. Science 5, 359(6371),

559 eaam7240. https://doi.org/10.1126/science.aam7240. 2018.

560 Brinkmann, T., Sartorius, D., Frimmel, F.H.: Photobleaching of humic rich dissolved organic matter.

561 Aquat. Sci. 65(4), 415–424. https://doi.org/10.1007/s00027-003-0670-9. 2003.

562 Brym, A., Paerl, H.W., Montgomery, M.T., Handsel, L.T., Ziervogel, K., Osburn, C.L.: Optical and

563 chemical characterization of base-extracted particulate organic matter in coastal marine

564 environments. Mar. Chem. 162(6), 96–113. https://doi.org/10.1007/s00027-003-0670-9. 2014.

565 Carlson, C.A., Hansell, D.A.: The contribution of dissolved organic carbon and nitrogen to

566 biogeochemistry of the Ross Sea. In: DiTullio, G., Dunbar, R. (Eds.), Biogeochemical Cycles in

567 the Ross Sea. AGU Press, Washington DC, pp. 123–142. 2003.

568 Carpenter, J.H.: The Chesapeake Bay Institute technique for the Winkler dissolved oxygen method.

569   Limnol. Oceanogr. 10(1964), 141–143. https://doi.org/10.4319/lo.1965.10.1.0141. 1964.

570   Catala, T.S., Reche, I., Fuenteslema, A., Romeracastillo, C., Nietocid, M., Ortegaretuerta, E.,

571   Alvarezsalgado, X.A.: Turnover time of fluorescent dissolved organic matter in the dark global

572   ocean. Nat. Com. 6(1), 5986–5993. https://doi.org/10.1038/ncomms6986. 2015.

573   Chen, Y., Yang, G., Xia, Q., Wu, G.: Enrichment and characterization of dissolved organic matter in

574   the surface microlayer and subsurface water of the South Yellow Sea. Mar. Chem. 182(Mar. 20),

575   1–13. https://doi.org/10.1016/j.marchem.2016.04.001. 2016.

576   Chowdhury, S.: Trihalomethanes in drinking water: Effect of natural organic matter distribution. Water

577   SA 39(1), 1–7. https://doi.org/10.4314/wsa.v39i1.1. 2013.

578   Coble, P.G.: Characterization of marine and terrestrial DOM in seawater using excitation-emission

579   matrix spectroscopy. Mar. Chem. 51(4), 325–346. https://doi.org/10.1016/0304-4203(95)00062-3.

580   1996.

581   Coble, P.G.: Marine optical biogeochemistry: the chemistry of ocean color. Chem. Rev. 107(2),

582   402–418. https://doi.org/10.1002/chin.200720265. 2007.

583   Cunliffe, M., Engel, A., Frka, S., Gasparovic, B., Guitart, C., Murrell, J.C., Wurl, O.: Sea surface

584   microlayers: A unified physicochemical and biological perspective of the air–ocean interface.

585   Prog. Oceanogr. 109(Feb.), 104–116. https://doi.org/10.1016/j.pocean.2012.08.004. 2013.

586   Danhiez, F.P., Vantrepotte, V., Cauvin, A., Lebourg, E., Loisel, H.: Optical properties of chromophoric

587   dissolved organic matter during a phytoplankton bloom. Implication for DOC estimates from

588   CDOM absorption. Limnol. Oceanogr. 62(4), 1409–1425. https://doi.org/10.1002/lno.10507.

589   2017.

590   Dragcevic, D., Pravdic, V.: Properties of the seawater-air interface. 2. Rates of surface film formation

591   under steady state conditions. Limnol. Oceanogr. 26, 492–499.

592   https://doi.org/10.1016/0198-0254(81)91185-7. 1981.

593   Duce, R.A., Hoffman, G.L., Ray, B.J., Fletcher, I.S., Wallace, G.T., Fasching, J.L., Piotrowicz, S.R.,

594   Walsh, P.R., Hoffman, E.J., Miller, J.M., Heffter, J.L.: Trace metals in the marine atmosphere:

595   Sources and fluxes, in: Marine Pollutant Transfer (H. L. Windom and R. A. Duce, eds.), pp.

596   77–119, Lexington Books, Lexington. 1976.

597   Engel, A., Galgani, L.: The organic sea-surface microlayer in the upwelling region off the coast of

598   Peru and potential implications for air–sea exchange processes. Biogeosciences 13(4), 989–1007.

599   https://doi.org/10.5194/bg-13-989-2016. 2016.

600   Frew, N.M., Bock, E.J., Schimpf, U., Hara, T., Hausecker, H., Edson, J.B., Jahne, B.: Air-sea gas

601   transfer: Its dependence on wind stress, small-scale roughness, and surface films. J. Geophys.

602   Res.-Oceans 109(C8), S17. https://doi.org/10.1029/2003JC002131. 2004.

603   Galgani, L., Engel, A.: Changes in optical characteristics of surface microlayers hint to

604   photochemically and microbially mediated DOM turnover in the upwelling region off the coast of

605   Peru. Biogeosciences 13(8), 2453–2473. https://doi.org/10.5194/bg-13-2453-2016. 2016.

606   Garrett, W.D.: Collection of slick-forming materials from the sea surface. Limnol. Oceanogr. 10(1965),

607   602–605. https://doi.org/10.2307/2833459. 1965.

608   Gonsior, M., Peake, B.M., Cooper, W.T., Podgorski, D., D'Andrilli, J., Cooper, W.J.: Photochemically

609   induced changes in dissolved organic matter identified by ultrahigh resolution fourier transform

610   ion cyclotron resonance mass spectrometry. Environ. Sci. Technol. 43(3), 698–703.

611   https://doi.org/10.1021/es8022804. 2009.

612   Grasshoff, K., Kremling, K., Ehrhardt, M.: Methods of Seawater Analysis, 3rd. Edition. pp. 407–420.

613   2007.

614   Guo, W., Yang, L., Zhai, W., Chen, W., Osburn, C.L., Huang, X., Li, Y.: Runoff-mediated seasonal

615   oscillation in the dynamics of dissolved organic matter in different branches of a large bifurcated

616   estuary-The Changjiang Estuary. J. Geophys. Res.-Biogeosciences 119, 776–793.

617   https://doi.org/10.1002/2013JG002540. 2014.

618 Hansell, D.A.: Dissolved organic carbon reference material program. Eos Transactions American

619   Geophysical Union, 86(35), 308. https://doi.org/10.1029/2005EO350003. 2013.

620 Hardy, J.T.: The sea surface microlayer: Biology, chemistry and anthropogenic enrichment. Prog.

621   Oceanogr. 11(4), 307–328. https://doi.org/10.1016/0079-6611(82)90001-5. 1982.

622 Hardy, J.T., Apts, C.W.: Photosynthetic carbon reduction: high rates in the sea-surface microlayer. Mar.

623   Biol. 101(3), 411–417. https://doi.org/10.1007/BF00428138. 1989.

624 Helms, J.R., Stubbins, A., Ritchie, J.D., Minor, E.C., Kieber, D.J., Mopper, K.: Absorption spectral

625   slopes and slope ratios as indicators of molecular weight, source, and photobleaching of

626   chromophoric dissolved organic matter. Limnol. Oceanogr. 53(3), 955–969.

627   https://doi.org/10.4319/lo.2008.53.3.0955. 2008.

628 Hoge, F.E., Vodacek, A., Blough, N.V.: Inherent optical properties of the ocean: retrieval of the

629   absorption coefficient of chromophoric dissolved organic matter from fluorescence measurements.

630   Limnol. Oceanogr. 38(7), 1394–1402. https://doi.org/10.4319/lo.1993.38.7.1394. 1993.

631 Jarvis, N.L.: Adsorption of surf ace-active material at the sea-air interface, Limnol. Oceanogr. 12,

632   213–221. https://doi.org/10.4319/lo.1967.12.2.0213. 1967.

633 Jørgensen, L., Stedmon, C.A., Kragh, T., Markager, S., Middelboe, M., Søndergaard, M.: Global

634   trends in the fluorescence characteristics and distribution of marine dissolved organic matter. Mar.

635   Chem. 126(1–4), 139–148. https://doi.org/10.1016/j.marchem.2011.05.002. 2011.

636   Kieber, D.J., Mcdaniel, J., Mopper, K.: Photochemical source of biological substrates in sea water:

637   implications for carbon cycling. Nature 341(6243), 637–639. https://doi.org/10.1038/341637a0.

638   1989.

639   Kok, M., Schouten, S., Sinninghe Damsté J.S.: Formation of insoluble, nonhydrolyzable, sulfur-rich

640   macromolecules via incorporation of inorganic sulfur species into algal carbohydrates. Geochim.

641   Cosmochim. Acta 64(15), 2689–2699. https://doi.org/10.1016/S0016-7037(00)00382-3. 2000.

642   Li, Y., He, Z., Yang, G., Wang, H., Zhuang, G.: Volatile halocarbons in the marine atmosphere and

643   surface seawater: Diurnal and spatial variations and influences of environmental factors. Atmos.

644   Environ. 214, 116820. https://doi.org/10.1016/j.atmosenv.2019.116820. 2019.

645   Liss, P.S., Duce, R.A.: The Sea Surface and Global Change, Cambridge University Press, 519. 1997.

646   Liss, P.S., Duce, R.A.: The Sea Surface and Global Change. Cambridge University Press: UK. 2005.

647   Liu, S.M., Qi, X.H., Li, X.N., Ye, H.R., Wu, Y., Ren, J.L., Zhang, J., Xu, W.Y.: Nutrient dynamics

648   from the Changjiang (Yangtze River) estuary to the East China Sea. J. Mar. Syst. 154(Feb.),

649   15–27. https://doi.org/10.1016/j.jmarsys.2015.05.010. 2016.

650   Liu, X., Beusen, A.H.W., Van Beek, L.P.H., Mogollón, J.M., Ran, X., Bouwman, A.F.: Exploring

651   spatiotemporal changes of the Yangtze River (Changjiang) nitrogen and phosphorus sources,

652   retention and export to the East China Sea and Yellow Sea. Water Res. 142(Oct. 1), 246–255.

653   https://doi.org/10.1016/j.watres.2018.06.006. 2018.

654   Margolin, A.R., Gonnelli, M., Hansell, D.A., Santinelli, C.: Black sea dissolved organic matter

655   dynamics: insights from optical analyses. Limnol. Oceanogr. 63(3), 1425–1443.

656   https://doi.org/10.1002/lno.10791. 2018.

657   Marie, D., Partensky, F., Jacquet, S., Vaulot, D.: Enumeration and cell cycle analysis of natural

658   populations of marine picoplankton by flow cytometry using the nucleic acid stain SYBR Green I.

659   Appl. Environ. Microbiol. 63(1), 186–193. https://doi.org/10.1109/50.337494. 1997.

660   Massicotte, P., Asmala, E., Stedmon, C., Markager, S.: Global distribution of dissolved organic matter

661   along the aquatic continuum: Across rivers, lakes and oceans. Sci. Total Environ. 609(Dec. 31),

662   180–191. https://doi.org/10.1016/j.scitotenv.2017.07.076. 2017.

663   Mcknight, D.M., Boyer, E.W., Westerhoff, P., Doran, P.T., Kulbe, T., Andersen, D.T.:

664   Spectrofluorometric characterization of dissolved organic matter for indication of precursor

665   organic material and aromaticity. Limnol. Oceanogr. 46(1), 38–48.

666   https://doi.org/10.4319/lo.2001.46.1.0038. 2001.

667   Medeiros, P.M., Seidel, M., Ward, N.D., Carpenter, E.J., Gomes, H.R., Niggemann, J., Dittmar, T.:

668   Fate of the Amazon River dissolved organic matter in the tropical Atlantic Ocean. Global

669   Biogeochem. Cycl. 29(5), 677–690. https://doi.org/10.1002/2015GB005115. 2015.

670   Mopper, K., Kieber, D.J.: Photochemistry and the cycling of carbon, sulfur, nitrogen and phosphorus.

671   In: Hansell DA, Carlson CA (eds) Biogeochemistry of dissolved organic matter. Academic Press,

672   San Diego, pp. 455–507. 2002.

673   Momzikoff, A., Brinis, A., Dallot, S., Gondry, G., Saliot, A., Lebaron, P.: Field study ofthe chemical

674   characterization of the upper ocean surface using various samplers. Limnol. Oceanogr. Methods

675   2(11), 374–384. https://doi.org/10.4319/lom.2004.2.374. 2004.

676   Nichols, C.M., Lardière, S.G., Bowman, J.P., Nichols, P.D., Gibson, J.A.E., Guézennec, J.: Chemical

677   Characterization of Exopolysaccharides from Antarctic Marine Bacteria. Microb. Ecol. 49(4),

678   578–589. https://doi.org/10.1007/s00248-004-0093-8. 2005.

679   Obernosterer, I., Catala, P., Reinthaler, T., Herndl, G.J., Lebaron, P.: Enhanced heterotrophic activity in

680   the surface microlayer of the Mediterranean Sea. Aquat. Microb. Ecol. 39(3), 293–302.

681   https://doi.org/10.3354/ame039293. 2005.

682   Ogawa, H., Amagai, Y., Koike, I., Kaiser, K., Benner, R.: Production of refractory dissolved organic

683   matter by bacteria. Science 292(5518), 917–920. https://doi.org/10.1126/science.1057627.

684   2001.

685   Orellana, M.V., Matrai, P.A., Leck, C., Rauschenberg, C.D., Lee, A.M., Coz, E.: Marine microgels as a

686   source of cloud condensation nuclei in the high Arctic. Proc. Natl. Acad. Sci. 108(33),

687   13612–13617. https://doi.org/10.1073/pnas.1102457108. 2011.

688   Ortega-Retuerta, E., Passow, U., Duarte, C.M., Reche, I.: Effects of ultraviolet B radiation on (not so)

689   transparent exopolymer particles. Biogeosciences 6(12), 3071–3080.

690   https://doi.org/10.5194/bg-6-3071-2009. 2009.

691   Osburn, C.L., Handsel, L.T., Mikan, M.P., Paerl, H.W., Montgomery, M.T.: Fluorescence tracking of

692   dissolved and particulate organic matter quality in a river-dominated estuary. Environ. Sci.

693   Technol. 46(16), 8628–8636. https://doi.org/10.1021/es3007723. 2012.

694   Parsons, T.R., Matia, Y., Lalli, C.M.: A Manual of Chemical and Biological Methods for Seawater

695   Analysis. Pergamon Press, Oxford. 1984.

696   Reinthaler, T., Sintes, E., Herndl., G.J.: Dissolved organic matter and bacterial production and

697   respiration in the sea-surface microlayer of the open Atlantic and the western Mediterranean sea.

698   Limnol. Oceanogr. 53(1), 122–136. https://doi.org/10.4319/lo.2008.53.1.0122. 2008.

699   Romera-castillo, C., Sarmento, H., Alvarezsalgado, X.A., Gasol, J.M., Marrase, C.: Production of

700   chromophoric dissolved organic matter by marine phytoplankton. Limnol. Oceanogr. 55(1),

701   446–454. https://doi.org/10.4319/lo.2010.55.1.0446. 2010.

702   Sabbaghzadeh, B., Upstill-Goddard, R.C., Beale, R., Pereira, R., Nightingale, P.D.: The Atlantic Ocean

703   surface microlayer from 50°N to 50°S is ubiquitously enriched in surfactants at wind speeds up to

704   13 m s^{-1}. Geophys. Res. Lett. 44(6), 2852–2858. https://doi.org/10.1002/2017GL072988. 2017.

705   Siegel, D.A.: Colored dissolved organic matter and its influence on the satellite‐based

706   characterization of the ocean biosphere. Geophys. Res. Lett. 32(20), 469–496.

707   https://doi.org/10.1029/2005GL024310. 2005.

708   Singh, S., D'Sa, E., Swenson, E.: Seasonal variability in CDOM absorption and fluorescence

709   properties in the Barataria Basin, Louisiana, USA. J. Environ. Sci. 22(10), 1481–1490.

710   https://doi.org/10.1016/S1001-0742(09)60279-5. 2010.

711   State Bureau of Technical Supervision Bureau, Specifications for Oceanographic Survey-Survey of

712   Biology in Sea Water. Standard Press of China, Beijing, pp. 17–20. 1992.

713   Stedmon, C.A., Bro, R.: Characterizing dissolved organic matter fluorescence with parallel factor

714   analysis: a tutorial. Limnol. Oceanogr.-methods 6(11), 572–579.

715   https://doi.org/10.4319/lom.2008.6.572b. 2008.

716   Stedmon, C.A., Markager, S.: Resolving the variability in dissolved organic matter fluorescence in a

717   temperate estuary and its catchment using PARAFAC analysis. Limnol. Oceanogr. 50(2),

718   686–697. https://doi.org/10.4319/lo.2005.50.2.0686. 2005.

719   Stedmon, C.A., Markager, S., Bro, R.: Tracing dissolved organic matter in aquatic environments using

720   a new approach to fluorescence spectroscopy. Mar. Chem. 82(3–4), 239–254.

721   https://doi.org/10.1016/s0304-4203(03)00072-0. 2003.

722   Stedmon, C.A., Markager, S., Tranvik, L., Kronberg, L., Slätis, T., Martinsen, W.: Photochemical

723   production of ammonium and transformation of dissolved organic matter in the Baltic Sea. Mar.

724   Chem. 104(3–4), 227–240. https://doi.org/10.1016/j.marchem.2006.11.005. 2007.

725   Su, Y., Hu, E., Feng, M., Zhang, Y., Chen, F., Liu, Z.: Comparison of bacterial growth in response to

726   photodegraded terrestrial chromophoric dissolved organic matter in two lakes. Sci. Total Environ.

727   579(Feb. 1), 1203–1214. https://doi.org/10.1016/j.scitotenv.2016.11.104. 2017.

728   Sun, H., Zhang, Y.H., Tan, S., Zheng, Y.F., Zhou, S., Ma, Q.Y., Yang, G.P., Todd, J., Zhang, X.H.:

729   DMSP-Producing Bacteria Are More Abundant in the Surface Microlayer than Subsurface

730   Seawater   of   the   East   China   Sea.   Microb.   Ecol.   80(1), 350–365.

731   https://doi.org/10.1007/s00248-020-01507-8. 2020.

732   Wang, F., Feng, T., Guo, Z., Li, Y., Lin, T., Rose, N.L.: Sources and dry deposition of carbonaceous

733   aerosols over the coastal East China Sea: Implications for anthropogenic pollutant pathways and

734   deposition. Environ. Pollut. 245(Feb.), 771–779. https://doi.org/10.1016/j.envpol.2018.11.059.

735   2019.

736   Weishaar, J.L., Aiken, G.R., Bergamaschi, B.A., Fram, M.S., Fujii, R., Mopper, K.: Evaluation of

737   specific ultraviolet absorbance as an indicator of the chemical composition and reactivity of

738   dissolved   organic   carbon.   Environ.   Sci.   Technol.   37(20),   4702–4708.

739   https://doi.org/10.1021/es030360x. 2003.

740   Weng, H., Tian, R., Ji, Z., Yu, X.: Potential relationships between atmospheric particulate matter

741   transported by winter monsoons and red tides in the East China Sea. Sci. Bull. 56(3), 297–305.

742   https://doi.org/10.1007/s11434-010-4209-x. 2011.

743   Woolf, D.K.: Bubbles and their role gas exchange, in The Sea Surface and Global Change, edited by P.

744   S. Liss and R. A. Duce, pp. 173–205, Cambridge Univ. Press, U. K. 2005.

745   Wotton, R.S., Preston, T.M.: Surface Films: Areas of Water Bodies That Are Often Overlooked.

746   Bioscience 55(2), 137–145. https://doi.org/10.1641/0006-3568(2005)055[0137:SFAOWB]2.0.CO.

747   2005.

748   Wurl, O., Wurl, E., Miller, L.A., Johnson, K., Vagle, S.: Formation and global distribution of

749   sea-surface microlayers. Biogeosciences 8(1), 121–135. https://doi.org/10.5194/bg-8-121-2011.

750   2011.

751   Wurl, O., Holmes, M.: The gelatinous nature of the sea-surface microlayer. Mar. Chem. 110(1–2),

752   89–97. https://doi.org/10.1016/j.marchem.2008.02.009. 2008.

753   Yamashita, Y., Hashihama, F., Saito, H., Fukuda, H., Ogawa, H.: Factors controlling the geographical

754   distribution of fluorescent dissolved organic matter in the surface waters of the Pacific Ocean.

755   Limnol. Oceanogr. 62(6), 2360–2374. https://doi.org/10.1002/lno.10570. 2017.

756   Yamashita, Y.: In situ production of chromophoric dissolved organic matter in coastal environments.

757   Geophys. Res. Lett. 31(14), 189–207. https://doi.org/10.1029/2004GL019734. 2004.

758   Yang, L., Zhang, J., Yang, G.P.: Mixing behavior, biological and photolytic degradation of dissolved

759   organic matter in the East China Sea and the Yellow Sea. Sci. Total Environ. 762(6), 143164.

760   https://doi.org/10.1016/j.scitotenv.2020.143164. 2020.

761   Yang, L., Zhuang, W., Chen, C.A., Wang, B., Kuo, F.: Unveiling the transformation and bioavailability

762   of dissolved organic matter in contrasting hydrothermal vents using fluorescence

763   EEM-PARAFAC.   Water   Res.   111(Mar.   15),   195–203.

764   https://doi.org/10.1016/j.watres.2017.01.001. 2017.

765   Zepp, R.G., Sheldon, W.M., Moran, M.A.: Dissolved organic fluorophores in southeastern US coastal

766   waters: correction method for eliminating Rayleigh and Raman scattering peaks in

767   excitation–emission   matrices.   Mar.   Chem.   89(1),   15–36.

768   https://doi.org/10.1016/j.marchem.2004.02.006. 2004.

769   Zhu, W.Z., Yang, G., Zhang, H.: Photochemical behavior of dissolved and colloidal organic matter in

770   estuarine and oceanic waters. Sci. Total Environ. s607–608(Dec. 31), 214–224.

771   https://doi.org/10.1016/j.scitotenv.2017.06.163. 2017.

Table 1 Spectral characteristics of the four fluorescent components identified by the PARAFAC

modal in this study, compared with those preciously identified.

Component	Ex$_{max}$ (nm)	Em$_{max}$ (nm)	Coble (1996)	Comparison with other studies using PARAFAC	Description and probable source
C1	345	455	peak C 320-360/420-480	Osburn et al. (2012)	Terrestrial-like humic substances
C2	255	310 (375)	peak A 230-260/380-460	Stedmon et al. (2003)	Tyrosine-like or marine humic-like substances
C3	315	385	peak M 290-310/370-420	Stedmon and Markager (2005)	Marine humic-like substances (biological degradation)
C4	280	335	peak T 270-280/340-350	Coble (1996)	Tryptophan-like; Non-Humic-like; Biological production in the water column

Table 2 Average temperature, salinity, wind speed, CDOM a(254), DOC, Chlorophyll-*a* (Chl-*a)*, dissolved oxygen (DO), $S_{275-295}$, S_R, and SUVA$_{254}$ of the SSW and SML in the YS and ECS during spring, summer, and winter.

		Spring		Summer		Winter	
	Water layer	mean	SD	mean	SD	mean	SD
Temperature (ºC)	SSW	14.0	4.91	24.0	3.66	14.0	5.23
Salinity	SSW	32.5	1.92	31.7	2.17	32.7	1.41
Wind Speed (m s^{-1})	SSW	5.98	2.86	5.47	2.51	6.09	2.52
DO (mg L^{-1})	SSW	6.44	0.85	7.57	1.07	8.32	0.99
Chl-*a* (µg L^{-1})	SSW	1.26	2.38	1.13	1.48	0.42	0.25
	SML	1.63	3.66	1.28	1.13	no data	
DOC (µmol L^{-1})	SSW	91.3	25.7	109.4	33.55	88.4	22.51
	SML	132.9	77.4	145.7	49.8	131.3	91.1
a(254) (m^{-1})	SSW	3.20	2.49	3.10	1.34	2.52	1.26
	SML	3.70	1.98	4.05	1.66	4.74	2.50
$S_{275-295}$ (nm^{-1})	SSW	0.0201	0.0049	0.0188	0.0035	0.0207	0.0068
	SML	0.0222	0.0073	0.0178	0.0021	0.021	0.0055
S_R	SSW	1.723	1.026	1.731	1.557	1.521	0.52
	SML	1.095	0.218	1.361	0.296	1.416	0.214
SUVA$_{254}$	SSW	2.067	0.664	2.244	0.671	3.008	0.949
(L mg-C^{-1} m^{-1})	SML	1.911	0.768	1.951	0.359	2.992	1.034

Table 3 Correlation coefficients between EF of DOM optical properties, Chl-a, DOC, PO_4^{3-}, NO_3^-, NO_2^-, SiO_3^{2-}, Cyanobacteria, Picophytoplankton, Bacterial abundance.

	EF of a(254)	EF of DOC	EF of Chl-a	Ef of C1	EF of C2	EF of C3	EF of C4	EF of PO_4^{3-}	EF of NO_3^-	EF of NO_2^-	EF of SiO_3^{2-}	EF of Cyanobacteria	EF of picophytoplankton
EF of DOC	0.185												
EF of Chl-a	0.092	0.021											
Ef of C1	**.336****	0.047	-0.119										
EF of C2	0.163	0.073	-0.017	**.635****									
EF of C3	**.413****	0.179	-0.096	**.907****	**.557****								
EF of C4	**.319****	0.021	0.011	**.574****	**.368****	**.628****							
EF of PO_4^{3-}	0.129	0.267	**.319***	0.131	-0.037	0.139	0.087						
EF of NO_3^-	-0.065	-0.054	0.235	-0.037	-0.044	-0.027	-0.053	0.26					
EF of NO_2^-	0.15	0.208	**.307***	0.142	-0.017	0.192	0.035	**.571****	0.271				
EF of SiO_3^{2-}	**.634***	0.004	0.074	0.122	-0.101	0.305	0.151	0.205	-0.118	-0.141			
EF of Cyanobacteria	0.091	-0.017	0.028	-0.027	-0.105	-0.047	-0.052	0.218	0.027	**.755****	-0.286		
EF of Picophytoplankton	**.347****	0.0281	0.252	-0.067	-0.082	-0.077	0.025	0.218	-0.08	0.113	-0.327	0.081	
EF of Bacterial abundance	-0.036	-0.069	-0.063	-0.061	0.004	0.014	-0.093	-0.12	-0.026	-0.073	-0.099	**.730****	-0.064

** Correlation is significant at the 0.01 level (two-tailed)

* Correlation is significant at the 0.05 level (two-tailed)